2008

Tropical-cyclone intensification and predictability in three dimensions

Nguyen, V. S

Tropical-cyclone intensification and predictability in three dimensions, Q. J. R. Meteorol. Soc., 134 (632), pp. 563-582: 2008, Nguyen, V. S., R. K. Smith, and M. T. Montgomery

QUARTERLY JOURNAL OF THE ROYAL METEOROLOGICAL SOCIETY
Q. J. R. Meteorol. Soc. **134**: 563–582 (2008)
Published online in Wiley InterScience
(www.interscience.wiley.com) DOI: 10.1002/qj.235

RMetS
ROYAL METEOROLOGICAL SOCIETY

Tropical-cyclone intensification and predictability in three dimensions

Nguyen Van Sang,[a] Roger K. Smith[a] and Michael T. Montgomery[b]*
[a] *Meteorological Institute, University of Munich, Germany*
[b] *Department of Meteorology, Naval Postgraduate School, Monterey, CA and NOAA Hurricane Research Division*

ABSTRACT: We present numerical-model experiments to investigate the dynamics of tropical-cyclone amplification and its predictability in three dimensions. For the prototype amplification problem beginning with a weak-tropical-storm-strength vortex, the emergent flow becomes highly asymmetric and dominated by deep convective vortex structures, even though the problem as posed is essentially axisymmetric. The asymmetries that develop are highly sensitive to the boundary-layer moisture distribution. When a small random moisture perturbation is added in the boundary layer at the initial time, the pattern of evolution of the flow asymmetries is changed dramatically, and a non-negligible spread in the local and azimuthally-averaged intensity results. We conclude, first, that the flow on the convective scales exhibits a degree of randomness, and only those asymmetric features that survive in an ensemble average of many realizations can be regarded as robust; and secondly, that there is an intrinsic uncertainty in the prediction of maximum intensity using either maximum-wind or minimum-surface-pressure metrics. There are clear implications for the possibility of deterministic forecasts of the mesoscale structure of tropical cyclones, which may have a major impact on the intensity and on rapid intensity changes.

Some other aspects of vortex structure are addressed also, including vortex-size parameters, and sensitivity to the inclusion of different physical processes or higher spatial resolution. We investigate also the analogous problem on a β-plane, a prototype problem for tropical-cyclone motion. A new perspective on the putative role of the wind–evaporation feedback process for tropical-cyclone intensification is offered also.

The results provide new insight into the fluid dynamics of the intensification process in three dimensions, and at the same time suggest limitations of deterministic prediction for the mesoscale structure. Larger-scale characteristics, such as the radius of gale-force winds and β-gyres, are found to be less variable than their mesoscale counterparts. Copyright © 2008 Royal Meteorological Society

KEY WORDS hurricane; tropical cyclone; typhoon; vortical hot towers; coherent structures; rapid intensification; predictability

Received 23 June 2007; Revised 14 February 2008; Accepted 19 February 2008

1. Introduction

There is a growing research literature on the role of asymmetric convection in all phases of tropical-cyclone life cycles, with special focus on convectively-induced asymmetries of rainfall and on the effects of various types of asymmetric vortex waves within the hurricane circulation. This research has led to an emerging view that many processes occurring within the tropical-cyclone core are manifestations of coherent structures that undergo their own life cycle and may ultimately decay in favour of the symmetric circulation.

Studies suggest that asymmetries arise in various ways. Many have focused on the effects of non-trivial vertical wind shear across a developing or mature vortex (e.g. Frank and Ritchie, 1999; Reasor *et al*., 2000; Frank and Ritchie, 2001; Black *et al*., 2002; Schecter and Montgomery, 2003; Rogers *et al*., 2003; Reasor *et al*., 2004); others have examined the structure of vortex-wave asymmetries supported by the vortex itself (Chen and Yau, 2001; Chen *et al*., 2003; Wang, 2002a, 2002b). The asymmetries can evolve into coherent sub-system-scale vortices that can persist for one or more revolutions about the parent vortex and induce significant intensity changes (e.g. Montgomery *et al*., 2002; Braun *et al*., 2006). Part of the intensity change observed in storms such as Danny (1997) (Blackwell, 2000), for example, may be due to the superposition of strong asymmetries, manifest as intense mesovortices, on the symmetric circulation. Supporting evidence comes from the Doppler-radar synthesis from Danny as well as earlier studies by, for instance, Marks and Houze (1984). Near-cloud-resolving numerical simulations of tropical storm Diana (1984) (Davis and Bosart, 2002; Hendricks *et al*., 2004) reveal convectively-induced mesovortices. The coherence of these structures is broadly consistent with the idea of 'hot towers', proposed almost five decades ago by Riehl and Malkus (1958) to explain the tropical overturning (Hadley) circulation, and revived recently to explain hurricane formation, intensification and evolution as observed in visible and infrared satellite data, lightning data, lidar data and high-resolution numerical models (Simpson *et al*., 1998;

* Correspondence to: Michael T. Montgomery, Department of Meteorology, Naval Postgraduate School, Monterey, CA, USA.
E-mail: mtmontgo@nps.edu

Montgomery and Enagonio, 1998; Möller and Montgomery, 2000; Enagonio and Montgomery, 2001; Heymsfield *et al*., 2001; Braun, 2002; Hendricks *et al*., 2004; Montgomery *et al*., 2006a). Collectively, the emerging concept is one of intensity and structural change (including warming in the eye) occurring through bursts, fundamentally stochastic in nature, associated with life cycles of asymmetries, rather than though a continuous 'slow' evolution connected with the axisymmetric secondary circulation.

The relationship between convectively-induced asymmetries and vertical wind shear has been usefully quantified through the concept of balanced lifting resulting from the presence of a lower-tropospheric vortex in shear. Building on the balanced-dynamical interpretations developed by Raymond and Jiang (1990) and Jones (1995), Frank and Ritchie (1999, 2001) have shown that mesoscale ascent achieves saturation in the lower troposphere and causes a shift of the rainfall from the downshear-right quadrant of the storm to the downshear-left quadrant. Trier *et al*. (2000) and Musgrave *et al*. (2008) have shown that balanced motion within a weak elevated baroclinic vortex functions in a similar way to focus rainfall and generate potential-vorticity (PV) anomalies. Such anomalies can merge to form a new centre; or a single, dominant anomaly can form a distinct centre and subsume the surrounding vortices. The mesovortices occur over a range of scales from 10 km to perhaps 100 km. The smaller ones resemble more the classical hot towers; the larger ones are mesoscale convective vortices, analogous to their cousins from continental convection (Rogers and Fritsch, 2001). Larger ones appear capable of forming a new centre; smaller vortices distort and can amplify an existing centre. Importantly, all such vortices share a common property of large cyclonic vorticity in the lower troposphere because of the vigorous organized convection that produced them in an already cyclonic-vorticity-rich environment. Thus, by vertical vortex-tube stretching near the ocean surface, they contribute vorticity to low levels of an existing vortex, or can form a low-level circulation by themselves. Either way, the emergent circulation becomes increasingly able to tap the latent reservoir of energy contained in the upper ocean by fluxes of enthalpy across the sea–air interface.

As a first step toward understanding the fluid dynamics of convective bursts and mesoscale vortices in incipient and mature cyclonic storms, a mechanism of vortex intensification by vortex Rossby waves (Montgomery and Kallenbach, 1997) was proposed, and investigated with a range of idealized numerical thought experiments that have provided important insights into the influence of convectively-induced PV asymmetries on the intensification of tropical storms. Montgomery and Enagonio (1998) and Möller and Montgomery (1999) carried out three-dimensional quasi-geostrophic and shallow-water balance-model experiments, respectively, with relatively high wave amplitudes, and identified a wave-induced eigenmode that interacts with the tropical-cyclone-like vortex. They hypothesized that the vortex can sustain the eigenmode, which itself can interact with convection and then feed back to the vortex. Subsequent studies by Möller and Montgomery (2000) and Enagonio and Montgomery (2001) confirmed the important role of convectively-induced asymmetric flow features in determining the structure and intensity of tropical cyclones. Simple 'axisymmetrization' experiments in three dimensions with monochromatic azimuthal-wave-number disturbances and single- and double-cluster PV anomalies show that vortex Rossby waves propagate both radially and vertically. When persistent convection is simulated by adding double-cluster PV anomalies to the PV fields, one after another (so-called 'pulsing'), a tropical storm intensifies to hurricane strength, with the final intensity dependent on the location and extent of the anomaly. The results support the existence of an alternative mode of tropical-cyclone intensification, different from the axisymmetric mode.

There have been numerous numerical studies of vortex amplification in the prototype problem for tropical-cyclone intensification, which considers the evolution of a prescribed, initially cloud-free, axisymmetric, baroclinic vortex on an f-plane. These studies can be divided into those using hydrostatic axisymmetric models with cumulus parametrization (e.g. Ooyama, 1969; Emanuel, 1989, 1995; Nguyen *et al*., 2002); those using hydrostatic three-dimensional models with cumulus parametrization (e.g. Zhu *et al*., 2001; Zhu and Smith, 2002, 2003); those using hydrostatic three-dimensional models with explicit microphysics (e.g. Wang 2001, 2002a, 2002b); and those using non-hydrostatic axisymmetric cloud models (e.g. Willoughby *et al*., 1984; Rotunno and Emanuel, 1987; Persing and Montgomery, 2003; Hausman *et al*., 2006). There have been also many studies of the analogous flow on a β-plane, which is a prototype problem for tropical-cyclone motion (e.g. Kurihara *et al*., 1990; Flatau *et al*., 1994; Dengler and Reeder, 1997; Wang and Holland, 1996a, 1996b) (There have been many more studies of this problem in a barotropic context, but our interest here is in baroclinic models with at least three vertical levels to represent the effects of deep convection.) It is significant that non-trivial flow asymmetries emerge in all the three-dimensional experiments, even those on the f-plane, and it is our opinion that a complete understanding of the intensification process in three dimensions is still lacking.

One of the primary goals of the present work is to seek a more complete understanding of the nature of the inner-core asymmetries and their role in tropical-cyclone intensification and motion. To achieve this objective, we employ high-resolution numerical experiments using the MM5 model to revisit the prototype intensification problem. In the main suite of numerical experiments, we choose the simplest explicit representation of moist processes that mimics pseudo-adiabatic moist thermodynamics. Using these benchmark experiments, we investigate the structure and evolution of the flow asymmetries and their impact on the vortex intensification and motion. A further goal is to investigate the predictability of the

DOI: 10.1002/qj

vortex intensity and asymmetric flow structure (Lorenz, 1969). In contrast to Lorenz (1969), the word 'predictability' is used here in a qualitative sense to describe the degree of randomness of the ensuing vortex evolution. It is reasonable to expect that the asymmetric flow structures are strongly influenced by deep convection, at least in the inner-core region, broadly defined as the region with radius less than twice the radius of maximum tangential wind speed at 900 hPa, just above the boundary layer. Since the pattern of deep convection is strongly influenced by the low-level moisture field, which is known to have significant variability on small space scales (e.g. Weckwerth, 2000), it is of interest to examine the variability of the inner-core asymmetries as a result of random variations in the boundary-layer moisture distribution. An investigation of this type is the subject of Sections 3 and 4.

2. The model configuration

The experiments described below are carried out using a modified version of the Penn State/NCAR fifth-generation Mesoscale Model (MM5 version 3.6) (Dudhia, 1993; Grell *et al*., 1995), which is suitable for the study of idealized problems. The model is configured with three domains: a coarse mesh of 45 km resolution, and two two-way-nested domains of 15 km and 5 km resolution. The domains are square, and are 5400 km, 1800 km and 600 km respectively on each side. For the experiments on the β-plane, the innermost domain moves to keep the vortex near the centre of the domain. There are 24 σ-levels in the vertical, 7 of which are below 850 hPa. One experiment employing a fourth domain (300 km square) has been conducted, to permit increased spatial accuracy down to 1.67 km horizontal grid spacing on the innermost domain. Another experiment employing higher vertical resolution (45 σ-levels) has been conducted also.

In order to keep the experiments as simple as possible, the main physics options chosen are the bulk-aerodynamic boundary-layer scheme (Braun and Tao, 2000) and the simplest explicit moisture scheme. These schemes are applied in all domains. The sea-surface temperature is set to a constant 27 °C. The initial vortex is axisymmetric, with a maximum tangential wind speed of 15 ms^{-1} at the surface at a radius of 135 km. The strength of the swirling wind decreases sinusoidally with height, vanishing at the top model level (50 hPa). The temperature field is initialized to be in gradient wind balance with the wind field, using the method described by Smith (2006). The far-field temperature and humidity are based on Jordan's Caribbean sounding during summertime conditions (Jordan, 1958), and are shown in a skew $T-\log p$ diagram in Figure 1.

Three main sets of experiments are carried out as detailed in Table I and Table II.

- The first (control) set is performed on an f-plane centred at 20 °N, and consists of a control experiment and ten additional ones in which the moisture fields throughout the innermost domain are randomly perturbed at low levels. The mixing-ratio perturbation lies between ± 0.5 g kg^{-1} at levels below 950 hPa. These experiments are carried out using a horizontal grid spacing of 5 km.
- The second set of experiments differs from the first set only in that they are performed on a β-plane.
- A third set is conducted on the f-plane. This allows us to assess:
  - the impact of evaporative cooling and related downdraught phenomenology on the intensification process simulated in the control set of experiments;
  - the extent to which a capped wind speed in the sea-to-air enthalpy interaction captures the intensification process in three dimensions (this helps us to discriminate between the contribution from the wind–evaporation feedback mechanism of wind-induced surface heat exchange (WISHE) (Rotunno and Emanuel, 1987; Emanuel, 1989), an essentially axisymmetric amplification process, and the horizontally-localized deep-convection organizational pathway, which has no axisymmetric counterpart (Montgomery *et al*., 2006a));
  - the robustness of the simulated intensification process to an increased horizontal resolution of 1.67 km.

The integration time for all experiments is 96 h. The results of the three sets of experiments are discussed in Sections 3, 4 and 5 respectively. In all analyses, the vortex centre is determined as follows: a 'first-guess' centre is determined by the minimum of the total wind speed at 900 hPa; then the centre is defined as the centroid of relative vorticity at 900 hPa over a circular region of 200 km radius around the first-guess centre. This method is less sensitive to asymmetric features than other methods (for example, determining the centre by minimum surface pressure), especially during the rapid-intensification phase when the system is highly asymmetric.

3. Experiments on an f-plane

3.1. Control f-plane experiment

3.1.1. Overview of vortex development

We describe first the development of the initial axisymmetric vortex in the control f-plane experiment (experiment C0 in Table I). Figure 2(a) shows time series of the minimum surface pressure and maximum total wind speed $VT_{\max}$ at 900 hPa (approximately 1 km high) during a 96 h integration. It shows also the maximum azimuthally-averaged tangential wind component at 900 hPa, $V_{\max}$, the average being taken about the centre defined in Section 2. As in many previous experiments, the evolution begins with a gestation period, during which the vortex slowly decays because of surface friction, but moistens in the boundary layer because of evaporation

DOI: 10.1002/qj

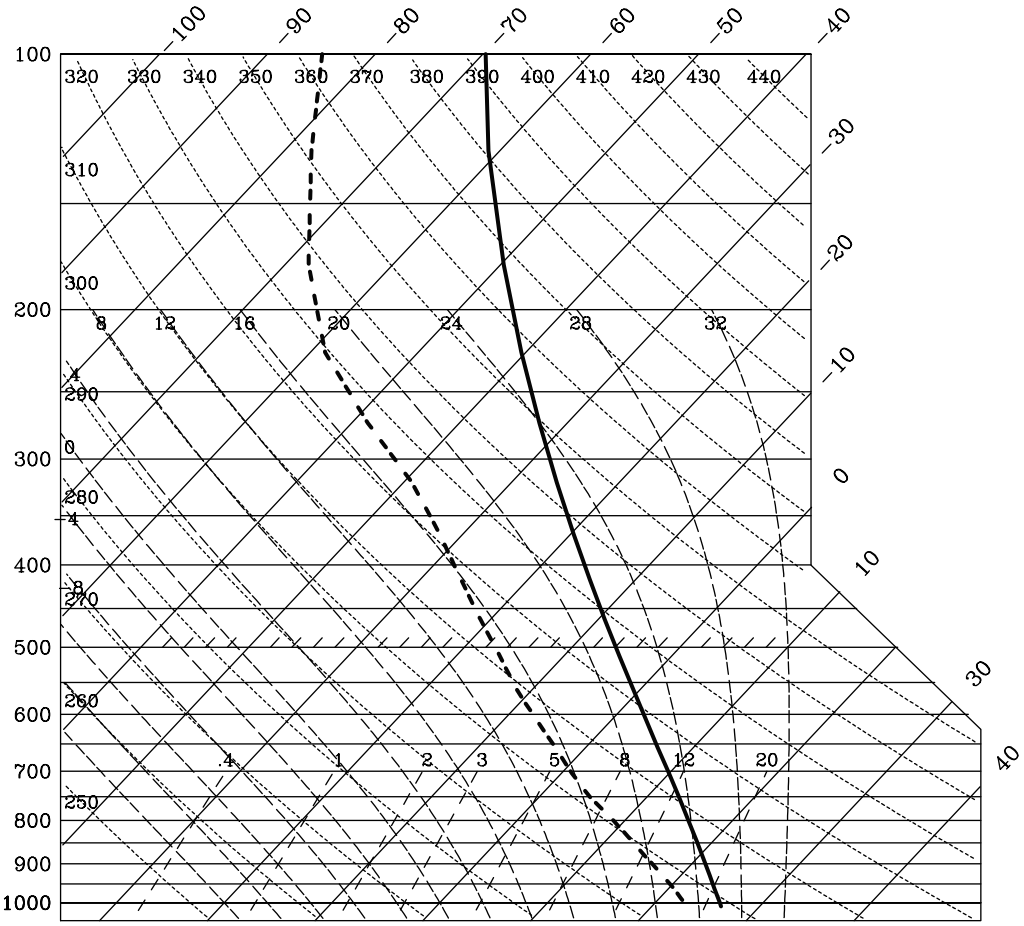

Figure 1. Skew T –log p diagram showing the temperature (solid line) and dew-point (dashed line) of the initial sounding at a radius of 2250 km from the domain centre.

Table I. Basic-physics experiments.

Symbol	Name	Description
C0	Control	Control experiment on an f-plane.
C1–C10	f-plane ensemble	Ten ensemble members. As C0, except that moisture fields below 950 hPa in domain 3 (5 km grid size) are disturbed by a value between ± 0.5 g kg^{-1}.
B0–B10	β-plane ensemble	As C0–C10, but on a β-plane.

Table II. Sensitivity experiments.

Symbol	Name	Description
S1	Radiative cooling	As C0, but includes the simple cooling option for the radiation scheme.
S2	Warm rain	As C0, but includes the warm-rain scheme.
S3	No heat flux	As C0, but the surface latent- and sensible-heat fluxes are set to zero.
S4	Capped heat flux	As C0, but the wind-speed dependence of the surface latent- and sensible-heat fluxes is suppressed beyond a wind speed of 10 ms^{-1}.
S5	High horizontal resolution	As C0, except that a fourth domain (300 km square) is added with a horizontal grid spacing of 1.67 km.
S6	High vertical resolution	As C0, except that the number of vertical levels is increased from 24 to 45.

DOI: 10.1002/qj

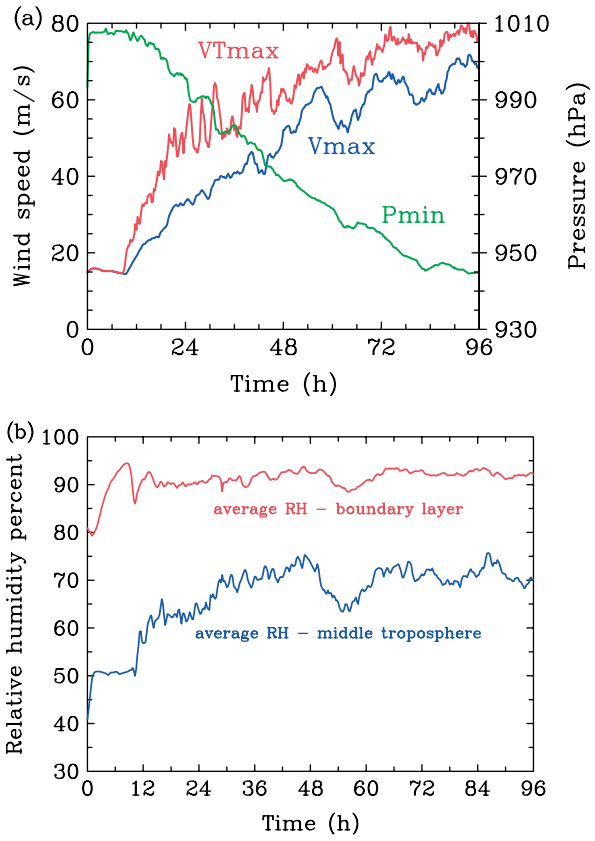

Figure 2. Vortex development in the f-plane control experiment C0. Time series of: (a) minimum surface pressure $P_{\min}$, maximum azimuthal-mean tangential wind component $V_{\max}$, and maximum total wind speed $VT_{\max}$ at 900 hPa; (b) average of relative humidity over a circular region of 100 km radius around the vortex centre in the ranges 900–1000 hPa (upper curve) and 400–700 hPa (lower curve).

from the underlying sea surface. This period lasts 9 h, during which time the minimum surface pressure rises from its initial value of 1004 hPa to 1008 hPa, but the maximum tangential wind speed decreases only slightly (by less than 0.5 ms^{-1}). The imposition of friction from the initial instant leads to inflow in the boundary layer and outflow above it, the outflow accounting for the decrease in tangential wind speed through the conservation of absolute angular momentum. The inflow is moist, and as it rises out of the boundary layer and cools, condensation progressively occurs in some grid columns interior to the corresponding radius of maximum tangential wind speed (Smith, 1968; Eliassen and Lystad, 1977). Existing relative vorticity is stretched and amplified in these columns, leading to the formation of localized rotating updraughts. Hendricks *et al.* (2004) and Montgomery *et al.* (2006a) have coined the term 'vortical hot towers' (VHTs) for these updraughts. As the updraughts develop, there ensues a period lasting about 45 h during which the vortex rapidly intensifies. During this time, $V_{\max}$ increases from approximately 14.5 ms^{-1} to approximately 60 ms^{-1}, while the minimum surface pressure decreases to 965 hPa. The average intensification rate is approximately 1 $\mathrm{ms}^{-1}\mathrm{h}^{-1}$. After 54 h, the minimum surface pressure continues to decline, reaching approximately 945 hPa at 82 h, after which it tends to a slightly smaller value at 96 h. The corresponding $V_{\max}$ increases only modestly, to approximately 68 ms^{-1} at 96 h, and the swirling wind field in the inner-core region may be regarded as quasi-steady for practical purposes after 72 h. Note that there are large fluctuations in $VT_{\max}$, up to 15 ms^{-1}, during the period of rapid intensification.

During the mature stage, the vortex exhibits many realistic features of a mature tropical cyclone, with spiral bands of convection surrounding an approximately symmetric eyewall and a central convection-free eye (details not shown).

3.1.2. *Relative humidity*

Following Bergeron (1950), recent work has hypothesized that a tropical depression vortex will begin to intensify only after the column-integrated relative humidity has become nearly saturated on the vortex scale (Rotunno and Emanuel, 1987; Emanuel, 1989; Bister and Emanuel, 1997; Raymond *et al.*, 1998). The basis for this idea originates in observations showing that regions of deep cumulus convection have adjacent downdraughts that advect mid-tropospheric air possessing a minimum of moist entropy into the boundary layer (e.g. Zipser and Gautier, 1978). Downdraughts originating near middle levels that manage to penetrate the boundary layer will dilute the high entropy content of the boundary layer, thereby rendering the lower troposphere less susceptible to deep convective activity and therefore to the buoyancy-induced convergence of angular momentum at low levels (Montgomery *et al.*, 2006a).

To investigate the potential relationship between the intensification simulated in the control experiment and the mid-tropospheric relative humidity (MRH), we have computed the average MRH in the range 400–700 hPa over a circular region of 100 km radius around the vortex centre. The time series of this average MRH is shown in Figure 2(b). The average MRH increases from its initial value of 40% to 50% in the first hour, and remains at this value for the next 8 h. When rapid intensification begins, at approximately 9 h, the average MRH increases from 50% to about 65% in 7 h. This is because when a grid box in the lower troposphere is saturated, latent heat is released, triggering deep convection. After 16 h, there is only a slight increasing trend, from 65% to 70% at the end of the simulation. Therefore the moistening of the middle layer in the control experiment accompanies the rapid increase of the tangential wind field; it does not precede it.

As described in the last section, the control experiment adopts the simplest explicit scheme available in MM5: as condensation occurs, the condensed water is immediately converted to precipitation and a commensurate amount of latent heat is released to the air; evaporative cooling and related downdraught phenomenology are neglected (pseudo-adiabatic dynamics). The explicit scheme in

DOI: 10.1002/qj

MM5 has been modified to add several more iterations (originally only one) to make the saturation temperature and saturation mixing ratio consistent at every grid point where condensation occurs. A more sophisticated experiment that incorporates the warm-rain process is discussed in Section 5. Although downdraughts are found to temper the intensification rate and reduce the simulated maximum sustained winds, the basic picture obtained from the simple scheme does not appear to be fundamentally different (not shown). The outcome of this experiment suggests that the control experiment broadly illustrates the nature of the vortex-intensification process.

3.1.3. Accumulated precipitation

It is of interest to determine the favoured regions of precipitation during the evolution. A high-precipitation region is a good indication of active updraughts on the system scale. Figure 3 shows 12 h accumulated precipitation at 12 h, 24 h, 48 h and 96 h. Although one finds accumulated rainfall over the entire region shown, the regions of high accumulated rainfall are concentrated around the core of the developing vortex. In the outer region and within the eye, the accumulated rainfall is less than 80 mm.

For the first 12 h, the accumulated precipitation is almost symmetric, and distributed in two separate rings at approximately 70 km and 100 km radius from the initial circulation centre. Early in the rapid-intensification period (24 h), the accumulated precipitation exhibits some asymmetry, manifest by localized anomalies within the precipitation annulus between 50 km and 70 km radius. Further into this period, at 48 h, the accumulated precipitation exhibits a wave-number-1 asymmetry, with the high rainfall found in three quadrants except the south-east sector of the vortex core (Figure 3(c)). Between 84 h and 96 h, the precipitation field contracts, and attains a distinct ring-like structure. The high precipitation annulus now occupies the region between 30 km and 60 km. A careful examination of the pattern of the accumulated precipitation of ensemble members (experiments C1–C10 in Table 1) and their mean at 48 h shows that, although there are large differences between precipitation patterns among the ensemble members, the mean accumulated-precipitation field is largely symmetric (not shown).

In order to obtain a deeper understanding of the physics of the intensification process in three dimensions, we turn now to examine the evolution of the vertical-velocity and relative-vorticity fields.

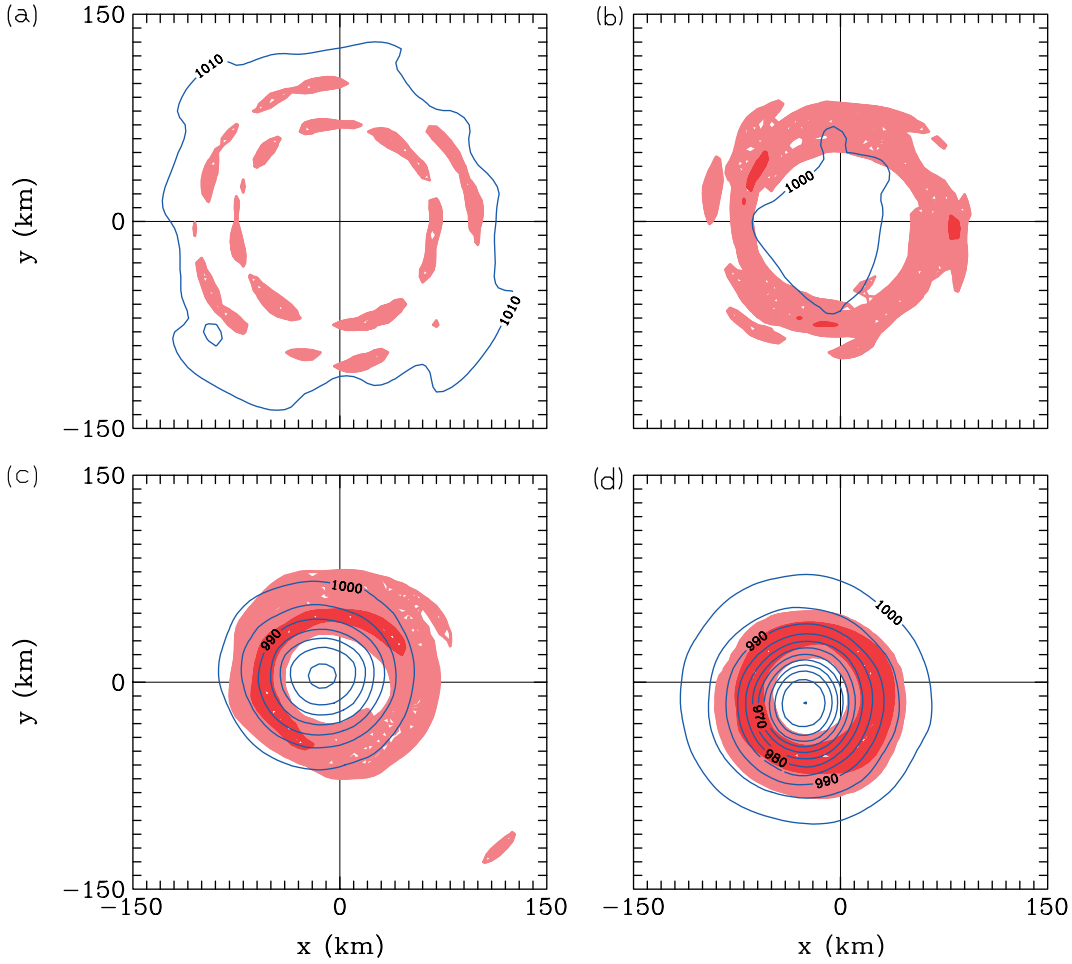

Figure 3. Surface pressure (contours, interval 5 hPa) and regions of 12 h accumulated precipitation exceeding 80 mm (40 mm in panel (a)), for the control experiment C0, at: (a) 12 h; (b) 24 h; (c) 48 h; (d) 96 h. Maximum precipitation amounts are approximately 200 mm in (a), 370 mm in (b), 440 mm in (c), and 530 mm in (d). Regions with values exceeding 300 mm are in dark red.

DOI: 10.1002/qj

3.1.4. *Vertical-velocity structure*

During the gestation period (0–9 h), there is only weak ascent at 850 hPa (above the boundary layer) in the vortex core region, within a radius of 150 km, and almost negligible ascent at 400 hPa (not shown). At 9 h, a narrow annulus of ascent is evident at 850 hPa, centred at 80 km radius, with a maximum value of approximately 0.7 ms^{-1} (not shown).

At the beginning of rapid intensification (9 h), latent-heat release by saturation in some grid boxes initiates deep convective cells. From 9 h to 9.75 h, the annulus of ascent evolves into distinct localized updraughts, with vertical-velocity maxima of 2–5 ms^{-1}. These updraughts extend to much higher levels, as shown in Figure 4(b), which illustrates their structure at 400 hPa. The distribution of the updraughts at 850 hPa shows a dominant azimuthal wave-number-14 pattern around the circulation centre. During the same period (9–9.75 h), a second annulus of upward motion, centred at a radius of 110 km, forms outside the first annulus; vertical-velocity maxima within it vary between 0.4 ms^{-1} and 1 ms^{-1}. Over the next 1.5 h (9.75–11.25 h), this outer ring of updraughts becomes dominant, and the two updraught rings interact and become irregular cells (not shown). These cells rotate cyclonically around the vorticity centroid, and are highly transient, with a convective lifetime on the order of one hour. The updraughts at 400 hPa are nearly above the updraught cores at 850 hPa throughout the intensification process. The extrema of upward velocity in the updraught cores at 400 hPa are typically two or three times greater than at the corresponding 850 hPa level.

From 11.25 h to the end of the rapid-intensification period (54 h), the updraughts increase in strength, with local peak values attaining approximately 22 ms^{-1} at 400 hPa between 16 h and 19 h (not shown). Two snapshots of the vertical motion are shown in Figure 4. The structure of these updraughts is still spatially irregular. During some periods, the upward motion occupies a contiguous region around the vortex centre (not shown). During rapid intensification, the number of intense updraughts decreases from twelve at 9 h to no more than three by the end of the period of rapid intensification. The intense cells contract inward over time, to a radius of approximately 35 km at 54 h. Evidence of spiral waves (gravity waves at speeds of approximately 40 ms^{-1}) propagating outwards is found throughout the vortex evolution (see, for example, Figure 4).

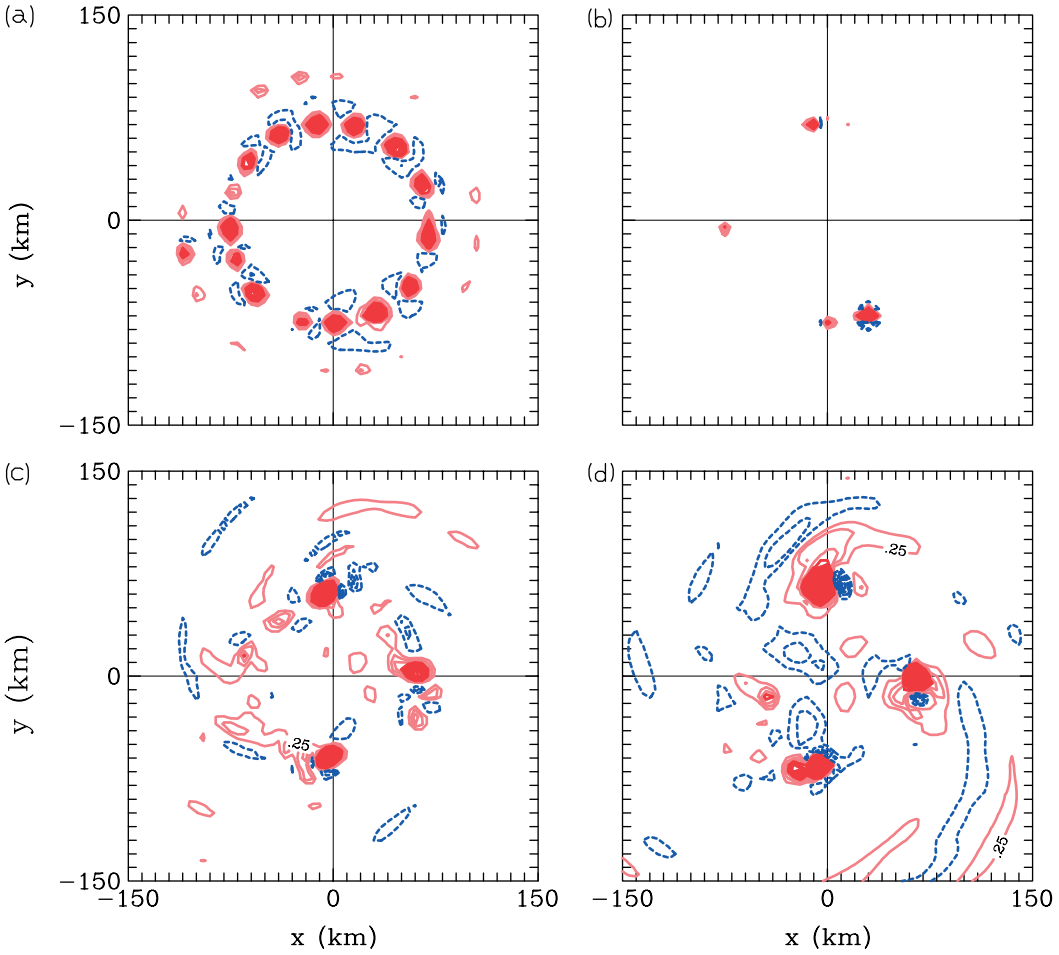

Figure 4. Vertical-velocity fields, in the control experiment C0, at (a,c) 850 hPa and (b,d) 400 hPa, after (a,b) 9.75 h and (c,d) 24 h. The contour interval is 0.25 ms^{-1}. Positive values are indicated by red solid contours (regions with values exceeding 1 ms^{-1} by dark red); negative values by blue dashed contours. The zero contour is not plotted.

DOI: 10.1002/qj

From approximately 54 h onward, the structure of concentrated upward motion shows various patterns over time, but is mainly monopolar, dipolar or tripolar, and always asymmetric.

3.1.5. Relative-vorticity structure

Snapshots of relative-vorticity fields are shown in Figures 5 and 6. The relative-vorticity structure changes only slightly during the first 9 h, retaining its initial monopolar structure. During this period, its value is approximately 4×10^{-4} s^{-1} at the centre of circulation. The updraughts that form at the beginning of the rapid-intensification period (9 h) tilt and stretch the local vorticity field. An approximate ring-like structure of intense small-scale vorticity dipoles quickly emerges (Figure 5(b,c,d)). This local dipolar structure in the relative vorticity occurs throughout the rapid-intensification period. The vorticity dipoles are highly asymmetric, with strong cyclonic vorticity anomalies and much weaker anticyclonic vorticity anomalies. Early in the intensification phase, the strong updraughts lie approximately in between the vorticity dipoles. Later in the intensification phase, strong updraughts are often approximately co-located with the strong cyclonic anomalies.

From approximately 12 h onwards, the VHTs are observed to grow horizontally in scale. This is due partly to merger and axisymmetrization with neighbouring cyclonic vorticity anomalies, and partly to convergence of same-sign vorticity from the nearby environment. During this time, the cyclonic anomalies move slowly inward, whereas the anticyclonic vorticity anomalies move slowly outward, decrease in amplitude, and undergo axisymmetrization by the parent vortex. Because this vorticity segregation process occurs in the presence of persistent mean near-surface inflow and low- to upper-level outflow, the segregation process cannot be explained simply by the mean advection associated with the diabatically-forced axisymmetric secondary circulation. A heuristic explanation of the segregation mechanism based on prior work is offered here as a first step towards a more detailed quantitative study.

Recall that vortex axisymmetrization involves the ingestion of same-sign vorticity anomalies, accompanied by the formation of same-sign vorticity filaments surrounding the parent vortex, as well as the expulsion of opposite-sign vorticity anomalies (Montgomery and Enagonio, 1998). During the merger phase, the amplitudes of the cyclonic vorticity anomalies are an order of magnitude higher than those of the background

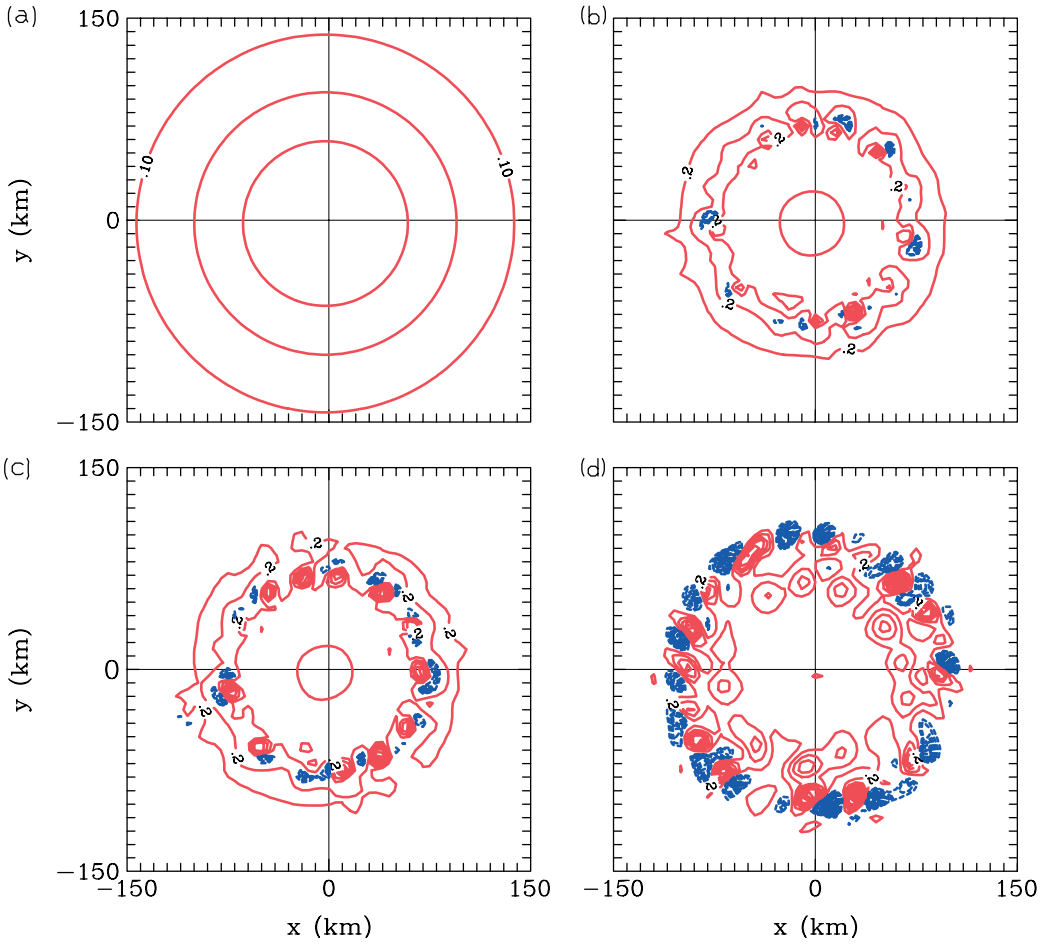

Figure 5. Vorticity fields, in the control experiment C0, at 850 hPa, after: (a) 0 h; (b) 9.75 h; (c) 10 h; (d) 12 h. Positive values are indicated by red solid contours, with a contour interval of 0.1×10^{-3} s^{-1} in (a) and 0.2×10^{-3} s^{-1} in (b)–(d). Negative values are indicated by blue dashed contours, with a contour interval of 0.5×10^{-4} s^{-1}. The zero contour is not plotted.

DOI: 10.1002/qj

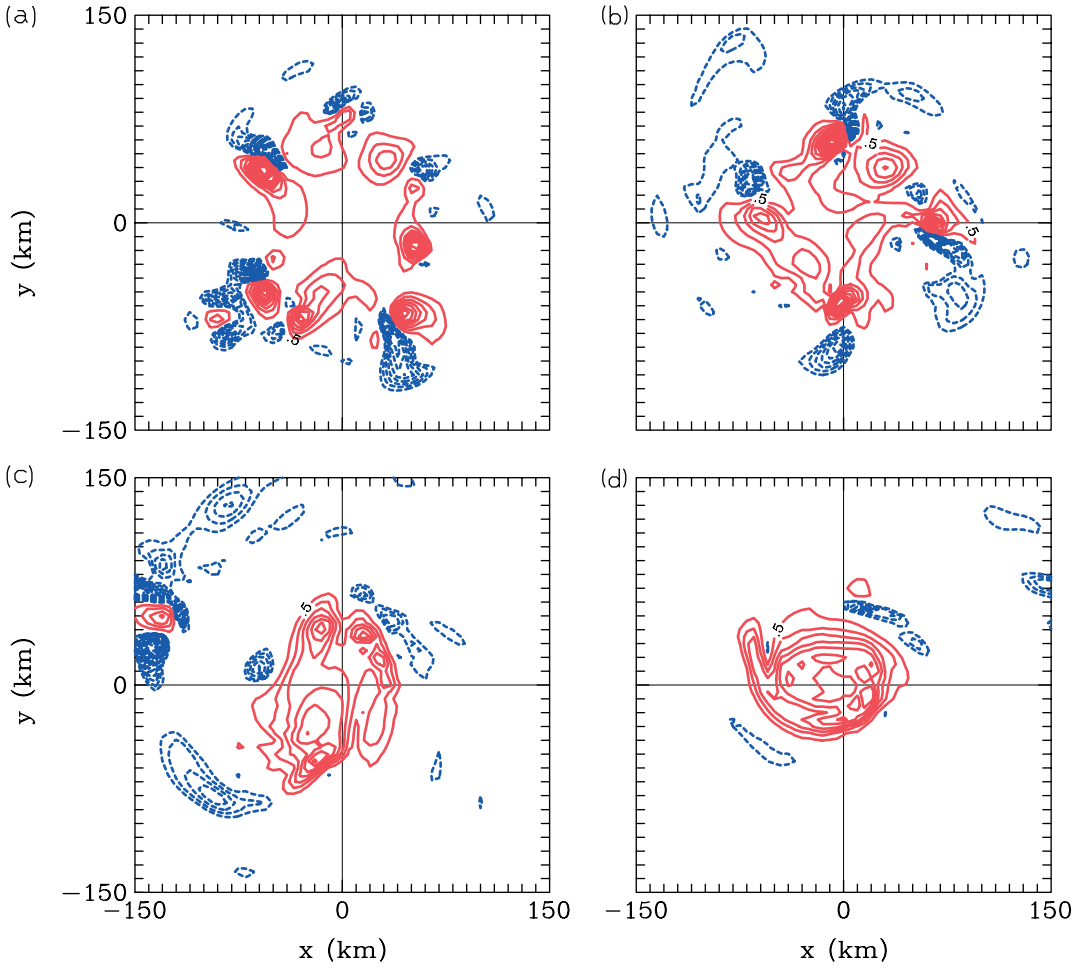

Figure 6. Vorticity fields, in the control experiment C0, at 850 hPa, after: (a) 18 h; (b) 24 h; (c) 36 h; (d) 48 h. Positive values are indicated by red solid contours, with a contour interval of 0.5×10^{-3} s^{-1}. Negative values are indicated by blue dashed contours, with a contour interval of 0.1×10^{-3} s^{-1} in (a)–(b) and 0.5×10^{-4} s^{-1} in (c)–(d). The zero contour is not plotted.

cyclonic vortex. Consequently, the cyclonic anomalies are not easily axisymmetrized by the parent vortex. However, since the initial vortex possesses a monotonic PV distribution, a related vortex-segregation mechanism is available. From vortex-motion theory (McWilliams and Flierl, 1979; Smith and Ulrich, 1990; Schecter and Dubin, 1999), intense cyclonic vorticity anomalies generally move 'up the ambient vorticity gradient', and vice versa for anticyclonic vorticity anomalies. Therefore intense cyclonic anomalies immersed in the negative vorticity gradient of the parent vortex will tend to move toward the centre, and anticyclonic anomalies will tend to move away from the centre. This segregation mechanism outweighs the low- to upper-level outflow and near-surface inflow. The divergent flow above the inflow layer weakens the anticyclonic anomalies, leaving them susceptible to axisymmetrization. The end result is that during rapid intensification the VHTs make a direct contribution to the system-scale spin-up (Montgomery *et al.*, 2006a), and a mesoscale inner-core region rich in cyclonic relative vorticity is constructed. By the end of the rapid-intensification period (from approximately 54 h), no more than three VHTs are active around the circulation centre (not shown). The evolution of the vortex after the merging phase is presumably well described by vortex Rossby waves and their coupling to the boundary layer and convection (Montgomery and Kallenbach, 1997; Chen and Yau, 2003; Wang, 2002a), but a more detailed analysis lies beyond the scope of this paper.

From the documented evolution of the vertical-velocity and relative-vorticity fields, it is clear that the VHTs dominate the rapid-intensification period at early times. A deeper, more quantitative investigation of the dynamics of the VHTs and vortex Rossby waves, and their contribution to the amplification of the system-scale vortex, will be presented in due course.

3.2. Ensemble experiments on an f-plane

In Section 3.1 it was shown that the flow asymmetries that develop in the control experiment during the period of rapid intensification are associated with the development of model deep-convective VHTs. Although these VHTs form more or less within an annular envelope where frictional convergence is a maximum (Smith, 1968; Eliassen and Lystad, 1977), their precise location

DOI: 10.1002/qj

in the annulus is determined by local asymmetries associated with the representation of an initially-symmetric flow on a square grid, which determine where grid-scale saturation first occurs. The symmetry would be expected to be broken also if random perturbations of moisture were present in the boundary layer. In reality, it is well known that moisture has significant variability on small spatial scales (e.g. Weckwerth, 2000). For this reason, it is important to investigate the sensitivity of the inner-core asymmetries to perturbations in the low-level moisture distribution. To do this, we have carried out an ensemble of experiments with an initially-perturbed moisture field at low levels (see Table I). The ensemble consists of ten members, in which the moisture fields are initially perturbed at all levels below 950 hPa. A random perturbation in the range ± 0.5 g kg^{-1} is added to the value of the moisture fields at every horizontal grid point in the innermost domain. This perturbation is different at different heights. The temperature fields are recalculated from the original virtual temperature fields to keep the mass fields unchanged. All other aspects of the model configuration are unchanged.

3.2.1. *Intensity and inner-core structure*

Figure 7(a) shows time series of the maximum of mean tangential wind speed of the control simulation and the ten-member ensemble. Mean wind maxima of all ensemble members are close to each other until approximately 13 h. From that time onwards, there is a spread in the simulated maxima. The spread occurs when the annular regions of high cyclonic relative vorticity of all members become irregular cells (not shown). The maximum difference between the mean intensities among all ensemble members at any given time over the whole simulation is approximately 15 ms^{-1}. All the ensemble simulations show the same rapid-intensification period, from 9 h to approximately 54 h, and a slight increasing trend in intensity from approximately 54 h onward.

Figure 7(b) shows the time series of maximum total wind speed $VT_{\max}$ for the same ensemble simulations. The spread in intensity occurs at approximately 10 h, sooner than the spread in mean tangential wind at approximately 13 h (Figure 7(a)). The maximum difference between the $VT_{\max}$ among all ensemble members at any given time over the whole simulation is approximately 20 ms^{-1}. During the first hour of rapid intensification (9–10 h), there is a steep increase in intensity for all ensemble members. Since this time interval coincides with the appearance of the ring-like structure of small-scale vorticity dipoles, $VT_{\max}$ is associated with the occurrence of VHTs. During the early phase of rapid intensification, the increase in $VT_{\max}$ occurs more rapidly and sooner than the increase of the maximum of mean tangential wind speed $V_{\max}$. This feature reflects the fact that the flow intensifies first on the convective scales (VHTs), and subsequently on the system scales.

Figure 7 also shows that after the gestation period, especially during the rapid-intensification phase, there is

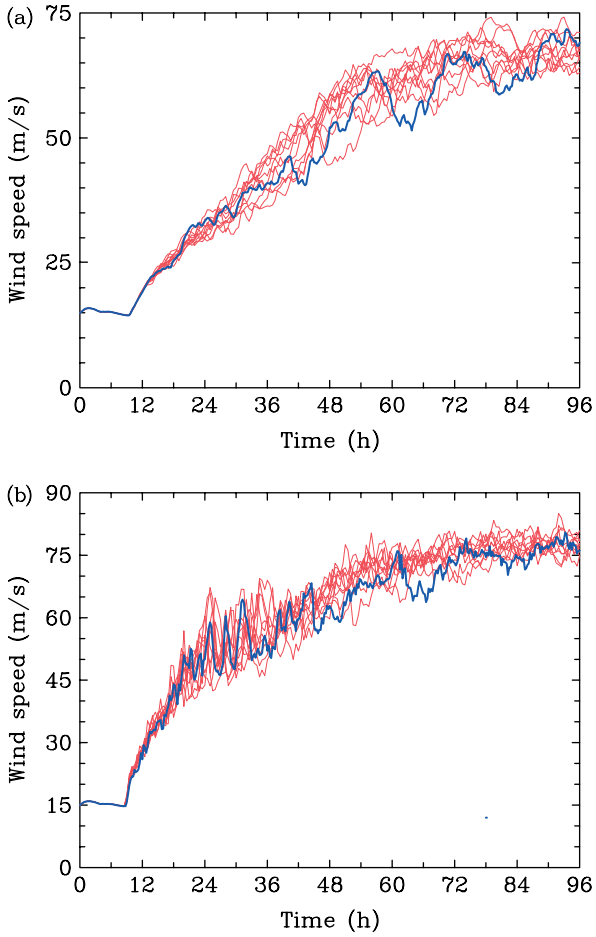

Figure 7. Time series, in the control experiment C0 (blue) and in the ten ensemble experiments C1–C10 (red), of: (a) azimuthal-mean maximum tangential wind speed; (b) maximum total wind speed at 900 hPa.

more variability between ensemble members in $VT_{\max}$ than in $V_{\max}$. These results have important operational implications, in that the local wind speed can change dramatically during rapid intensification.

Inspection of the relative-vorticity fields of individual ensemble members shows similar characteristics to those in the control experiment. The relative-vorticity field is not axisymmetric, and the detailed pattern of small-scale vorticity structure is significantly changed. Figure 8 illustrates this point at a typical time during the rapid-intensification process. We conclude that the ensuing evolution of VHTs exhibits a degree of randomness, and is highly sensitive to the moisture distribution in the boundary layer. For all ensemble members, the vertical velocity is dominated by VHTs (see Figure 9).

3.2.2. *Vortex-size parameters*

We investigate now the development of two critical parameters relating to the vortex size: the radius of maximum azimuthally-averaged tangential wind speed (RMW), and the radius of gale-force wind (RGW). (In general usage, 'gale-force wind' refers to a sustained

DOI: 10.1002/qj

wind speed of at least 17 ms^{-1}.) The former provides a scale for the region of extreme winds and for the eye size. The latter provides a scale for the region of potential significant damage.

Figure 10 shows time series of the RMW and RGW in experiments C0–C10. During the gestation period, the RMW expands from its initial value of 135 km to approximately 147 km, but after 5 h it starts to decrease rapidly. There is a spread in the RMW between ensemble members beginning with the rapid-intensification period (9–54 h – see Figure 2). There is a large variation in the RMW during this period, the difference between ensemble members reaching a maximum of approximately 32 km at 28 h. From 54 h onward, the RMW curves tend asymptotically to a mean value of 35 km, and the maximum difference among the ensemble members is approximately 7 km at 96 h.

The development of the radius of maximum total wind speed exhibits similar characteristics (not shown), but the variation among ensemble members is high during the rapid-intensification period. This is mainly because of the unpredictable and locally-intense circulations associated with the VHTs (see Section 3.1). The difference in the radius of maximum *total* wind speed among ensemble members reaches its maximum of approximately 70 km at 19 h, and decreases to approximately 17 km at 96 h.

The maximum mean wind speed of all ensemble members exceeds gale force at approximately 12 h. The RGW is calculated from that time onward by taking the outer radius at which the azimuthal-mean tangential wind speed equals 17 ms^{-1}. As shown in Figure 10, the RGW quickly increases between 12 h and 15 h. After that time, the RGW continues to grow for all ensemble members. From 24 h to 72 h, the variation is approximately 15 km. From 72 h onward, the variation is smaller (approximately 5 km), and there is an approximately-linear increase with time for all ensemble members. Thus all of the simulated hurricanes exhibit a real growth in horizontal size after the inner-core has reached a quasi-steady state.

From the results shown, it appears that the spread of the RMW and RGW decreases as the vortex approaches its quasi-steady maximum intensity. The spreads of maximum tangential wind speed and total wind speed diminish a little with time, and tend asymptotically to a value comparable in a relative sense to the spread in the RMW. This result indicates that the RGW for the mature

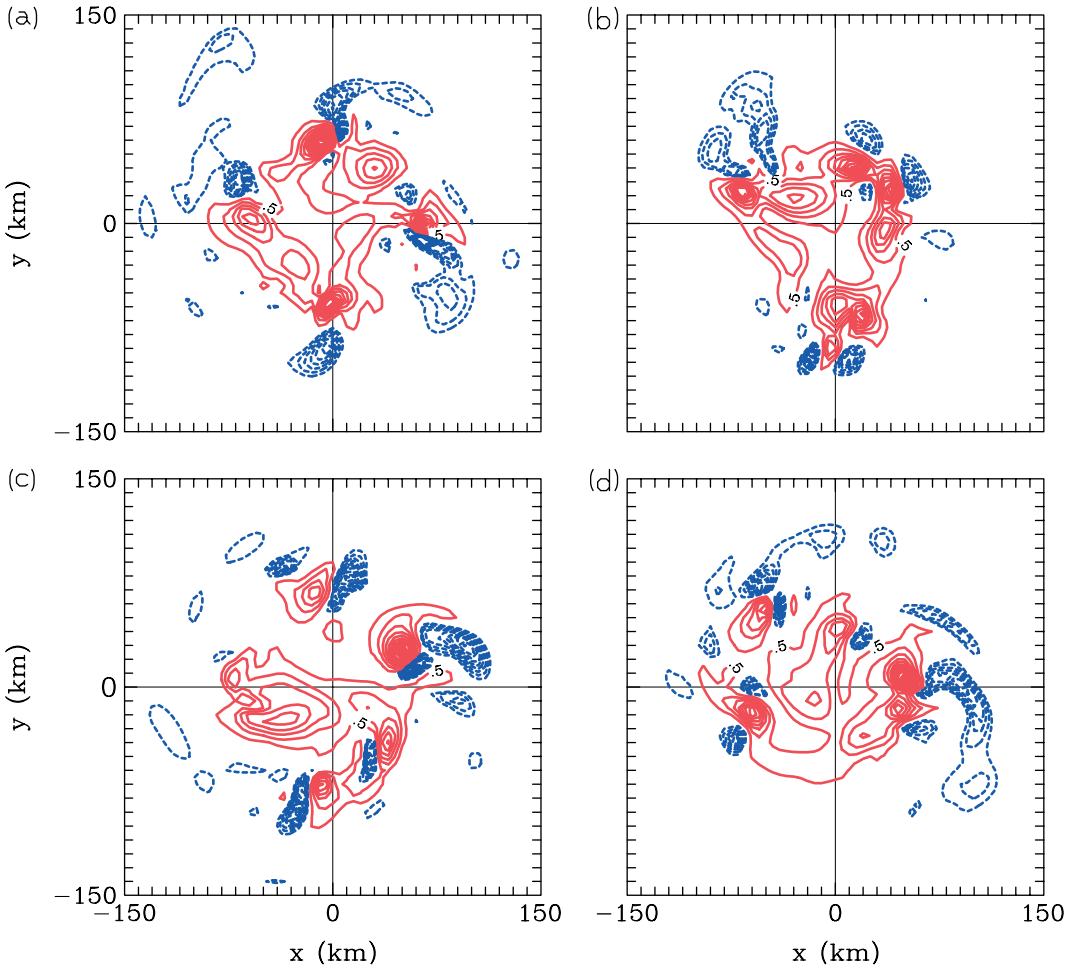

Figure 8. Relative-vorticity fields of (a) the control experiment C0, and (b,c,d) three representative realizations from the f-plane ensemble at 24 h. Positive values are indicated by red solid contours, with a contour interval of 0.5×10^{-3} s^{-1}. Negative values are indicated by blue dashed contours, with a contour interval of 0.1×10^{-3} s^{-1}. The zero contour is not plotted.

DOI: 10.1002/qj

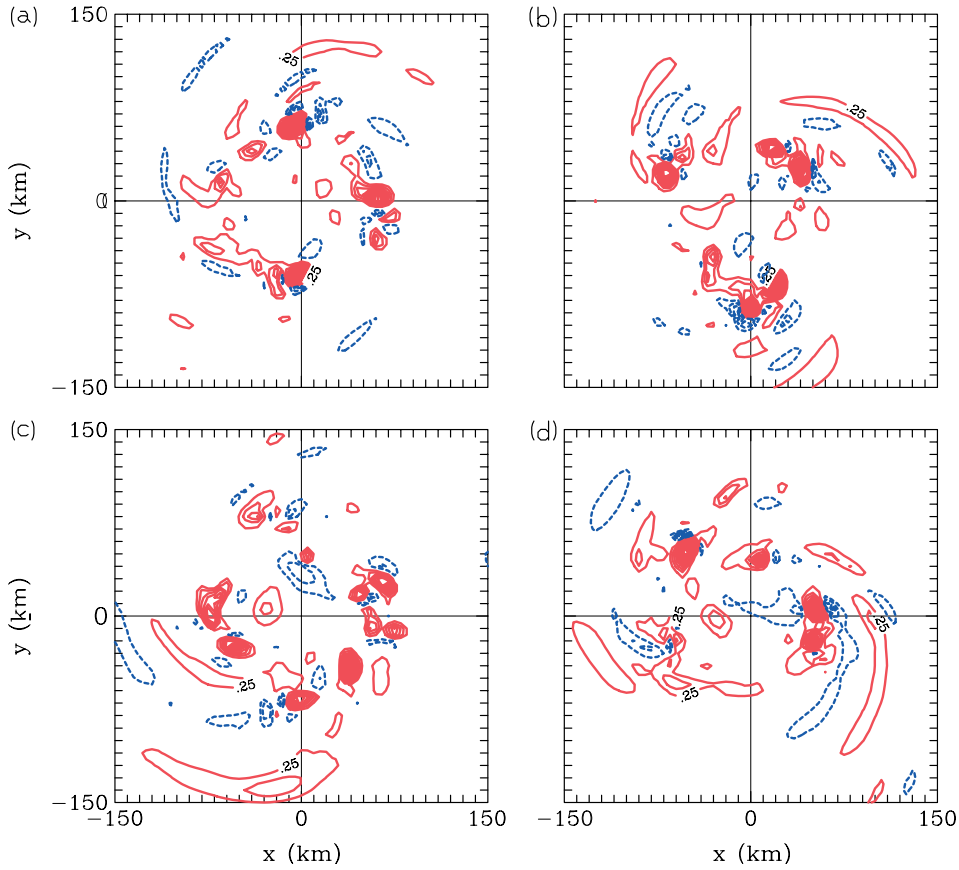

Figure 9. Vertical-velocity fields of (a) the control experiment C0, and (b,c,d) three representative ensemble experiments at 24 h. The contour interval is 0.25 ms^{-1}. Positive values are indicated by red solid contours; negative values by blue dashed contours. The zero contour is not plotted.

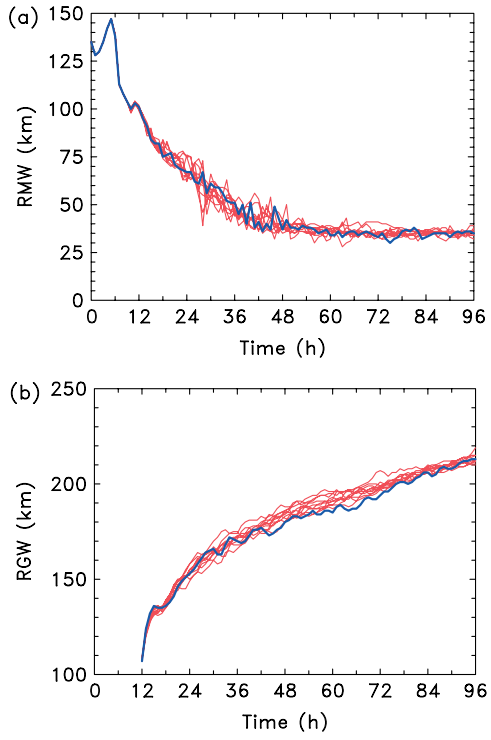

Figure 10. Time series, for experiments C0 (blue) and C1–C10 (red), of: (a) radius of maximum mean tangential wind speed; (b) radius of gale-force wind.

storm has less variability than, for example, V_{max} or the RMW.

4. Experiments on a β-plane

In the last section we showed that on an f-plane, the flow asymmetries that evolve are highly sensitive to the initial moisture distribution. Partly because of the practical connection between hurricane track and storm-scale asymmetries, it is of interest to enquire whether a similar result is true when there is a mechanism to force the asymmetries, such as occurs on a β-plane or when a vortex is exposed to vertical wind shear in its environment. To investigate this question, we have repeated all the above experiments on a β-plane (see Table I). The effects of vertical wind shear will be investigated in a future paper.

Although the vortex moves north-northwest as a result of the β effect, and the fields of accumulated precipitation are much more asymmetric than in the f-plane experiments (not shown), the main characteristics in the vortex-core region are unchanged, and the rapid-intensification period is dominated by the VHTs.

It was shown in the last section that there is about a 15 ms^{-1} spread in mean intensity of the ensemble members. The asymmetric forcing implied by the presence

DOI: 10.1002/qj

of β may be expected to produce an effect on the initial pattern of convective cells similar to a moisture perturbation. In order to determine whether there is a significant difference between the f- and β-plane experiments, one must compare the average of the ensemble means; it is insufficient just to compare two deterministic experiments. Figure 11(a) shows the ensemble average of the azimuthally-averaged tangential wind speed at 900 hPa as a function of time, for the f-plane experiments C0–C10 and the β-plane experiments B0–B10. The curves lie close to each other for approximately 60 h, after which time, the average $V_{\max}$ for the f-plane experiments becomes slightly stronger than that for the β-plane (but no more than 4 ms^{-1}). In particular, the differences lie well inside the intervals of the largest difference between any two members of either f-plane or β-plane ensemble experiments (indicated by the vertical bars). The spread found in the β-plane set is comparable to that in the f-plane case. Figure 11(a) shows also the time-series of the ensemble average of the corresponding $VT_{\max}$. For the duration of the experiments, the two curves are nearly coincident, suggesting similar magnitudes of VHTs on either the f-plane or β-plane. A similar diagram for minimum surface pressure is shown in Figure 11(b). It is clear that there is practically no difference between the minimum surface pressure for the f-plane and β-plane cases. On the basis of these results, we conclude that the β effect has essentially no impact on the maximum intensity of the vortex during the course of the simulations (Our results differ profoundly from those of Kwok and Chan (2005), Wu and Braun (2004) and Peng *et al.* (1999) with regard to the influence of β on the simulated vortex intensity in the long term. Those studies found that β caused significant weakening (on the order of 15 to 20 ms^{-1}), but they were limited by considerably coarser horizontal resolution and parametrized convection).

In order to investigate the predictability of the vortex motion on the β-plane, the vortex centres of the experiments B0–B10 are calculated, as discussed in Section 2. The results are shown in Figure 12. The tracks start to spread after approximately 12 h. The maximum difference in relative position between any two members increases with time, and is approximately 60 km at 96 h. The 60 km spread in the vortex tracks by day four provides a useful estimate of the track uncertainty associated with moisture perturbations in the boundary layer.

To confirm our expectation of the influence of the β-effect on the large-scale environment (e.g. Fiorino and Elsberry, 1989; Smith and Ulrich, 1990; Smith and Weber, 1993), we consider the horizontal vorticity asymmetries of the ensemble experiments B0–B10 on all three domains. A combined multiple-grid configuration of domains 1 (45 km grid size) and 2 (15 km grid size) is set up as follows. First domain 1 is interpolated to 15 km resolution, and then domain 2 is projected onto the interpolated domain 1 where the data from domain 2 are defined. The vorticity asymmetry is calculated at each output time on the combined domains 1 and 2 by subtracting the axisymmetric relative vorticity from the

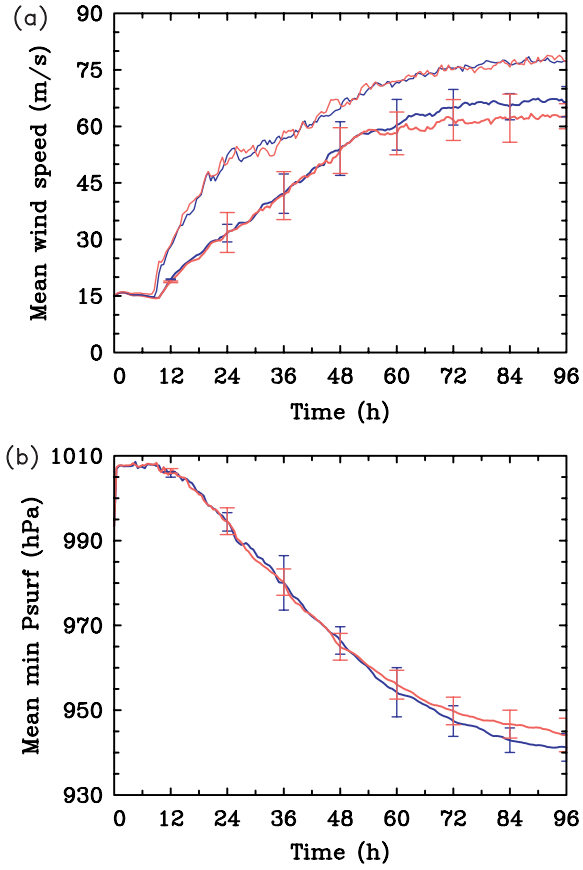

Figure 11. Ensemble-average time series, for the f-plane experiments C0–C10 (blue line) and the β-plane experiments B0–B10 (red line), of: (a) azimuthally-averaged tangential wind speed (two lower curves) and the maximum local wind speed (two upper curves); (b) minimum surface pressure. The vertical bars indicate the maximum differences among ensemble members.

total relative vorticity. Because the innermost domain moves during the integration process, the inner-core asymmetries represented on domain 3 (5 km grid size) are calculated separately and then projected onto the asymmetries of the combined domains 1 and 2 within 250 km from the vortex centre.

Figure 13 shows the ensemble-mean vorticity asymmetries of the β-plane experiments B0–B10 on the 850 hPa surface at 48 h. In the inner-core region, the ensemble-average asymmetry does not show a dominant wavenumber-1 pattern. This has been verified at other times (not shown). For scales larger than the vortex's RMW, the pattern of the mean relative-vorticity asymmetry has distinct β-gyres appearing at a radius of about 500 km from the vortex centre, and the magnitude of these vorticity gyres is on the order of 10^{-5} s^{-1}. A β-gyre consists of a spiral band of cyclonic relative vorticity to the southwest of the vortex centre and an anticyclonic relative-vorticity band to the northeast. The standard deviation of the relative-vorticity asymmetry between ensemble members (not shown) is only appreciable within a radius of 200 km, and is negligible (less than 10^{-6} s^{-1}) outside this radius. We attribute this variability to the VHTs. In fact, the large-scale β-gyres are virtually the same among all ensemble members.

DOI: 10.1002/qj

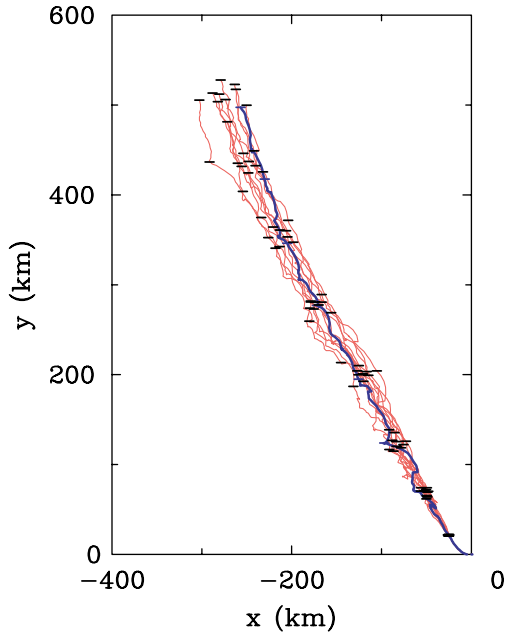

Figure 12. Vortex tracks for the β-plane experiments B0–B10. Tick marks are shown on the tracks for every 12 h interval. The track of experiment B0 is shown in blue.

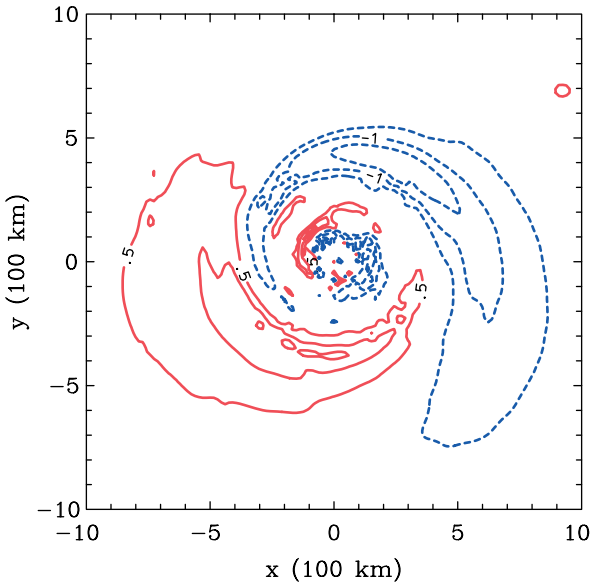

Figure 13. Ensemble-mean relative-vorticity asymmetry of the β-plane experiments B0–B10 at 850 hPa after 48 h. The contour interval is 0.5×10^{-5} s^{-1} in the range $\pm 5 \times 10^{-5}$ s^{-1}. Positive values are indicated by red solid contours; negative values by blue dashed contours. The zero contour is not plotted.

Our conclusions in this section differ profoundly from those of a recent paper by Ritchie and Frank (2007). They compared two deterministic experiments of a similar type to ours, using a similar version of MM5 with 5 km horizontal resolution. They found that the vortex on the β-plane 'quickly develops a persistent wave-number-1 asymmetry in its inner core'. From our ensemble experiments, we question the validity of this conclusion. Unfortunately, it is not possible to compare the details of vortex evolution in our control experiments with theirs, as they show only coarse-grained, horizontal fields of PV, and only at the mature stage of vortex development. Nevertheless, they did find little difference in intensity between their f- and β-plane experiments, consistent with our findings.

5. Sensitivity experiments

The control experiment described in Section 3.1 is chosen to be as simple as possible, the main physics parametrizations being the bulk-aerodynamic boundary-layer scheme and a very simple explicit moisture scheme. Other potentially important processes, such as evaporative downdraughts and radiative cooling, are omitted. Here, we describe six additional experiments in which the sensitivity of vortex evolution to the inclusion of additional physical effects and to higher horizontal resolution is investigated. These experiments are detailed in Table II.

The first experiment, S1, explores the effects of radiative cooling, using a simple scheme in which the temperature T in degrees Celsius is reduced everywhere by an amount $0.017T + 1.8$ per day (In an experiment with no initial vortex, this scheme produces scattered convection after approximately three days. Therefore this radiation scheme is not ideal for long-term simulations of a tropical cyclone; however, it should be adequate for assessing the basic influence of radiation on time-scales of approximately three days or less.).

The second experiment, S2, includes a warm-rain scheme, in which cloud water and rainwater are predicted explicitly in clouds. In this scheme, microphysical processes are represented by an empirical auto-conversion function that converts cloud water to rainwater. The rainwater falls with a terminal velocity that is a function of the mixing ratio for rainwater, and it evaporates when the relative humidity falls below 100%. The cooling associated with the evaporation leads to resolved-scale downdraughts. Details of the scheme as coded in MM5 can be found in Grell *et al.* (1995) and Hsie *et al.* (1984).

Two further experiments are designed to examine the role of surface fluxes. In experiment S3, no sensible- or latent-heat fluxes are allowed, while in experiment S4, there is an upper bound of 10 ms^{-1} on the wind speed in the formulae from which the sensible- and latent-heat fluxes are calculated.

All the above experiments have the same domain configuration as the control experiment C0. Experiment S5 includes a fourth, innermost, domain with a 1.67 km horizontal grid spacing. Experiment S6 employs higher vertical resolution.

With radiative cooling included (experiment S1), rapid intensification occurs about 2 h earlier than in the control experiment C0 (see Figure 14). This is because with radiative cooling the temperature of a grid column is slightly reduced, so that grid-scale saturation occurs a little earlier. However, during the period of rapid intensification, the intensification rate is similar to that

DOI: 10.1002/qj

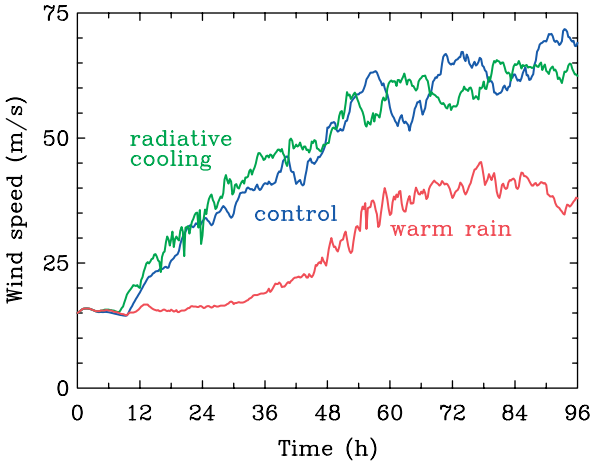

Figure 14. Time series of azimuthal-mean maximum tangential wind speed at 900 hPa, in the control experiment C0 and in the experiments with a representation of radiative cooling (S1) or warm-rain processes (S2).

in the control experiment. In the mature stage, the vortex intensity is higher than that of the control experiment for some periods and lower for others. The developing vortex is found to be qualitatively similar to that in the control experiment, in that the asymmetries are still dominated by similar-strength VHTs, but differ in detail in the same way as experiments C1–C10 differ from C0 (see Figure 15(a,b)). We conclude that radiative cooling does not change the qualitative picture of the vortex evolution for the duration of the model integration.

When warm-rain processes are included (experiment S2 – see Figure 14), rapid intensification is delayed, and the vortex intensifies more slowly than in the control experiment. On a time-scale of four days, the mature-stage intensity is also lower than in C0, the peak maximum azimuthal-mean tangential wind being approximately 45 ms^{-1} at 77 h, compared with 63 ms^{-1} at this time in C0. An extended run of S2 was carried out to determine the final maximum intensity at this resolution. At 384 h, the maximum mean tangential wind is approximately 53 ms^{-1}. We attribute this behaviour to a reduction in the convective instability that results from convectively-driven downdraughts associated with the rain process and due to the reduced buoyancy in clouds on account of water loading. The VHTs emerge from approximately 10.5 h, and are irregular and transient during the period 12–36 h. The merging and axisymmetrization processes start later than in C0, from about 36 h to 60 h. The local extremes of relative vorticity are typically less than in C0 (see, for example, Figure 15(c)), although the qualitative characteristics of the intensification period are similar.

When the surface latent- and sensible-heat fluxes are suppressed entirely (experiment S3), the vortex does not intensify (see Figure 16), even though there is some transient hot-tower convection and local wind-speed enhancement. The VHTs emerge at approximately 20 h, but then rapidly decrease in strength before they have the opportunity to merge (not shown). The local peak wind speed shows a slow decrease with time: this behaviour is consistent with decaying VHTs that rapidly consume pre-existing convective available potential energy (CAPE) by convection and receive no replenishment from latent-heat fluxes in the boundary layer.

When the wind-speed dependence of the surface latent- and sensible-heat fluxes is capped at a wind speed of 10 ms^{-1} (experiment S4), the evolution of maximum mean tangential wind is similar but generally less than that in the control experiment (see Figure 16). Nevertheless, the difference between the two never exceeds 15 ms^{-1} at any time. The intensification process is still dominated by VHTs. The maximum VHT strength has approximately the same amplitude as in the control experiment during the intensification process (see Figure 15(d)). On the system scale, late into the intensification period and in the mature state, the vorticity anomalies are slightly weaker than in the control experiment. From this evidence, we conclude that the intensification is due not to pre-existing CAPE, but rather to the modest replenishment of boundary-layer θ_e by sea-to-air latent-heat fluxes. This is an important finding because it demonstrates that a positive feedback between water-vapour flux and cyclonic wind speed is not essential for tropical-cyclone intensification and maintenance, as proposed by Rotunno and Emanuel (1987) in their axisymmetric experiments. This result has been found to be robust to the inclusion of cloud water and evaporatively-cooled downdraughts (not shown). It has been confirmed also in a rerun at high spatial and temporal resolution of Rotunno and Emanuel's (1987) experiment J with speed-capped sea-to-air fluxes of latent and sensible heat (capping also the coefficients of exchange of latent and sensible heat) (J. Persing, personal communication). It is informative to point out that the heat and momentum exchange coefficients are independant of wind speed for the bulk-aerodynamic boundary-layer scheme in MM5 (e.g., Braun and Tao, 2000). These and other aspects of the capped-wind-speed flux experiments, as well as a deeper examination of the differences between the three-dimensional and axisymmetric intensification mechanisms, will be reported in forthcoming work.

In the high-horizontal-resolution experiment (S5), the smaller grid spacing enables grid-scale saturation to occur sooner. This is reflected in the fact that rapid intensification begins at about 6 h, 3 h earlier than in the control experiment (Figure 17). The mature-stage intensity is higher than in the control, with $V_{\max}$ approximately 70 ms^{-1} at 54 h and 80 ms^{-1} at 96 h. The RMW during the mature stage is approximately 30 km, slightly less than that of the control experiment (approximately 35 km). The maximum *local* wind speed $VT_{\max}$ approaches 90 ms^{-1} at 96 h. From these results there is clear evidence of an increase in intensity with increased horizontal resolution. The tendency of the simulated intensity to increase substantially at higher resolution has been documented in the literature (Persing and Montgomery, 2003; Hausman *et al.*,

DOI: 10.1002/qj

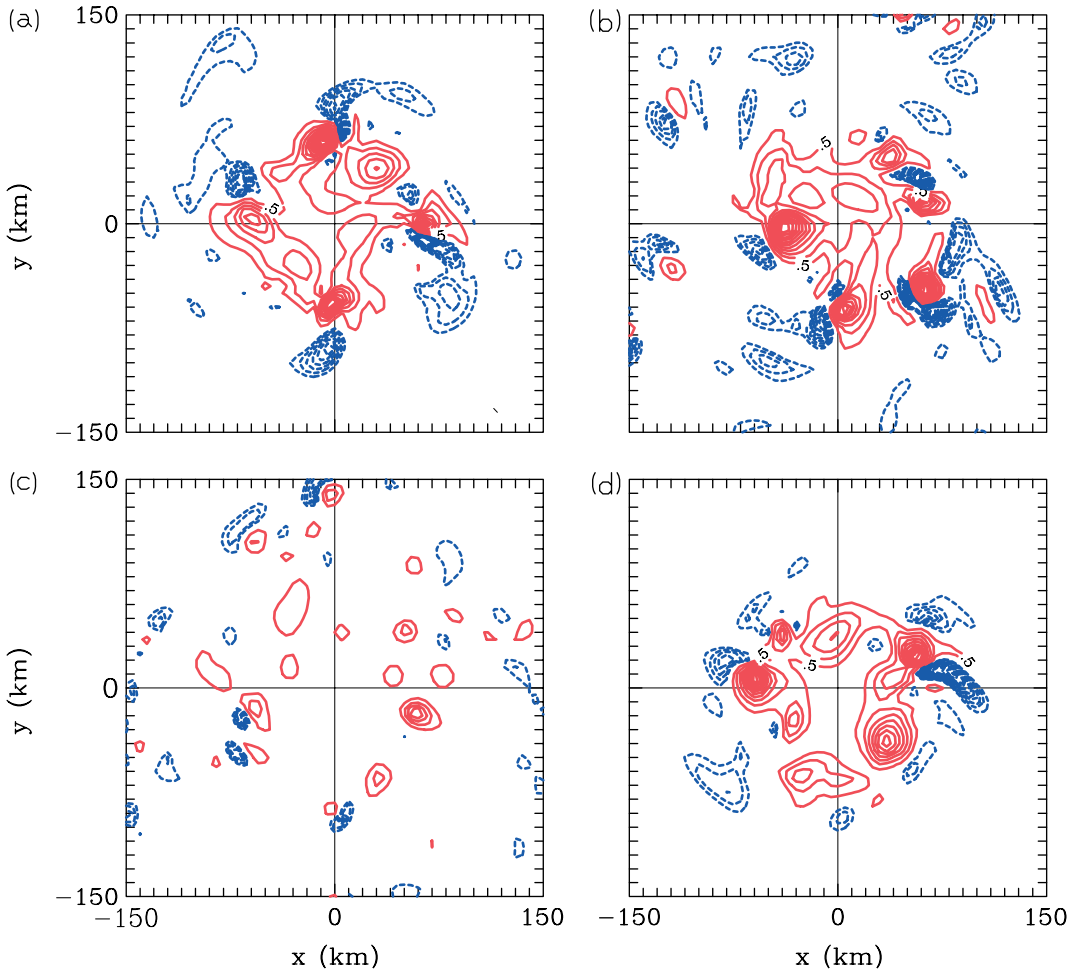

Figure 15. Vorticity fields at 850 hPa, after 24 h, for: (a) control experiment C0; (b) radiative cooling S1; (c) warm rain S2; (d) capped heat flux S4. Positive values are indicated by red solid contours, with a contour interval of 0.5×10^{-3} s^{-1}. Negative values are indicated by blue dashed contours, with a contour interval of 0.1×10^{-3} s^{-1}. The zero contour is not plotted.

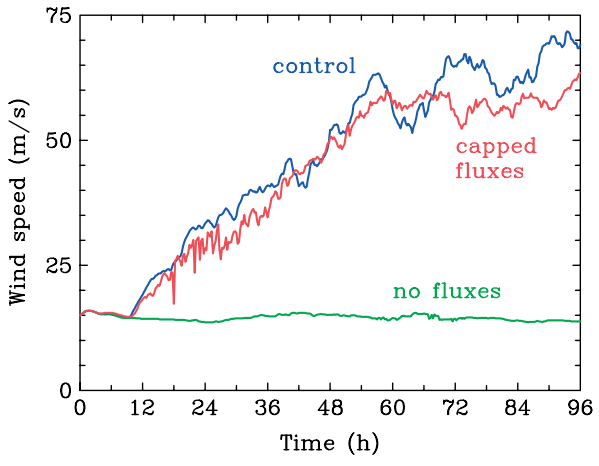

Figure 16. Time series of azimuthal-mean maximum tangential wind speed at 900 hPa, in the control experiment C0 and in the experiments with capped surface fluxes (S4) or no surface fluxes (S3). In the experiments with capped surface fluxes, the wind-speed dependence of both latent- and sensible-heat fluxes is suppressed for wind speeds exceeding 10 ms^{-1}.

2006), but a detailed examination of this issue in three dimensions is beyond the scope of this work (This simulated hurricane and that of the control experiment have been confirmed to be 'superintense' as defined by Persing and Montgomery (2003). These numerical experiments support the hypothesis that the superintensity phenomenon persists in three dimensions (Montgomery *et al*., 2006b).).

At the beginning of rapid intensification in experiment S5 (Figure 18(a)), many more VHTs form in an annular region than in the control experiment. (The increased number and reduced horizontal scale of the initial towers are consistent with the well known tendancy of convective instability to favour the smallest scales). Nevertheless, the behaviour of VHTs during the intensification phase is similar to that in C0, the ensemble experiments and the physics-sensitivity experiments, with cyclonic-vorticity skewness in the lower troposphere, segregation of cyclonic and anticyclonic vorticity anomalies, axisymmetrization of anticyclonic vorticity anomalies, and ultimately the establishment of a mesoscale inner-core region rich in cyclonic vorticity (see, for example, Figure 18(c)). After the VHT segregation-and-merger phase subsides (from approximately 50 h onward), a distinct eyewall forms, with an approximate ring of enhanced cyclonic

DOI: 10.1002/qj

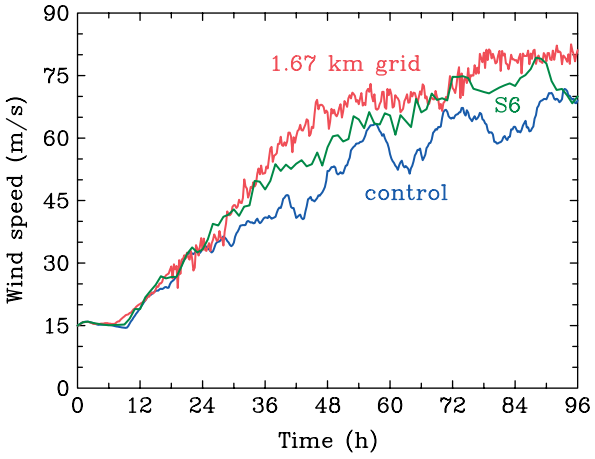

Figure 17. Time series of azimuthal-mean maximum tangential wind speed at 900 hPa: in the control experiment C0; in the experiment S5 with an increased horizontal grid resolution of 1.67 km in a fourth, innermost, domain; and in the experiment S6 with the number of vertical levels increased to 45.

vorticity (Figure 18(d)). (In this sense, the control results at 5 km horizontal grid spacing have not yet converged.) This eyewall structure persists beyond this time. Vorticity patterns in the eyewall region take a variety of forms, including pentagons, squares, triangles, ellipses and circles. Complete breakdown of the eyewall is not observed, however (cf. Schubert *et al*., 1999). The evolution is consistent with the picture of propagating near-discrete and sheared vortex Rossby waves and localized mixing events between the eyewall and its interior and exterior.

One candidate explanation for the persistence of an elevated vorticity ring is that the sustained convergence of the secondary circulation acts to temper the shear instability that has been demonstrated previously in unforced hurricane-like vortices (Montgomery *et al*., 2002; Nolan, 2001; cf. Kossin and Schubert, 2001; Schubert *et al*., 1999). In a complementary study, it has also been suggested that the cloudiness that pervades hurricane eyewalls tempers these shear instabilities (Schecter and Montgomery, 2007). These explanations are not mutually exclusive, and a deeper study of this topic will be presented in due course.

We have carried out also a high-vertical-resolution experiment (S6), in which the horizontal resolution is

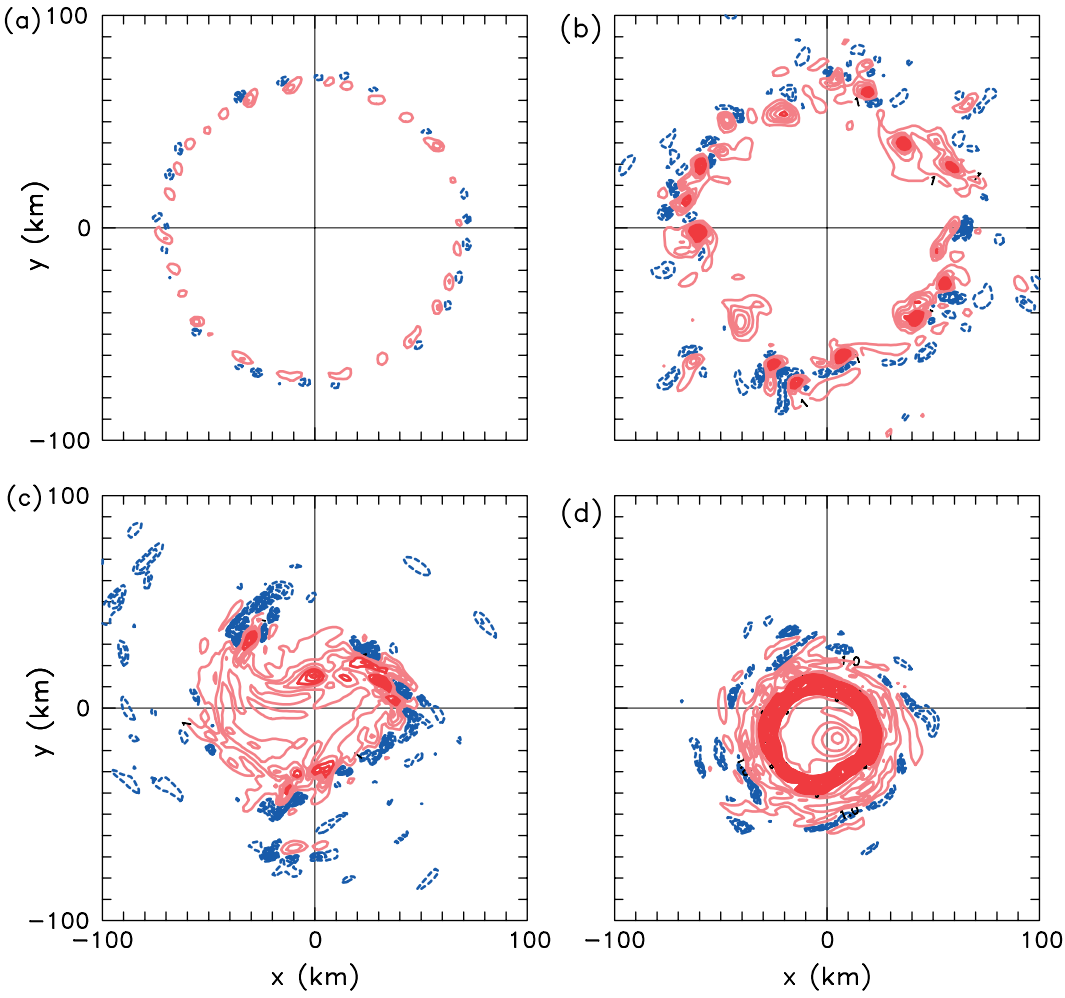

Figure 18. Vorticity fields at 850 hPa, for 1.67 km experiment (S5), after: (a) 7 h; (b) 18 h; (c) 36 h; (d) 78 h. Positive values are indicated by red solid contours, with a contour interval of 10^{-3} s^{-1}. Regions with values exceeding 5×10^{-3} s^{-1} are indicated by dark red contours. The zero contour is not plotted. Negative values are indicated by blue dashed contours, at intervals of 0.5×10^{-3} s^{-1} in (a)–(b) and 0.2×10^{-3} s^{-1} in (c)–(d).

DOI: 10.1002/qj

unchanged from experiment C0, but the number of vertical levels is increased from 24 to 45. The additional vertical levels are added so that the interval in σ is half that of the control experiment in every vertical interval except the lowest two (because the vertical resolution there is already sufficient). Figure 17 shows that the mean vortex in experiment S6 is generally more intense than in the control C0. We believe that the reason for this is the increased resolution of the region where the inflow turns upwards and flows radially outwards to the eyewall, which more accurately represents the moist entropy flux from the low-level eye into the eyewall. This low-level-eye air possesses higher equivalent potential temperature than air found at the RMW, because of the lower surface pressure and non-zero surface winds, and contributes additional heat and local buoyancy to the eyewall. The net result is an enhancement of the radial gradient of equivalent potential temperature above the inflow layer, which supports strong tangential winds, in accordance with axisymmetric thermal wind balance above the boundary layer (Montgomery *et al*., 2006b, appendix). We have verified that the evolution in S6 is similar to that presented for the experiment C0. These findings confirm the dominance and intrinsic randomness of the VHTs during the intensification phase (Kimball and Dougherty (2006) have examined the sensitivity of idealized hurricane structure and development to the distribution of vertical model levels, and found also that vortex intensity is sensitive to this distribution. Our calculations here show that the basic intensification process is independent of the vertical resolution.).

To summarize, in the sensitivity experiments the vortex evolution during the merger phase is dominated by VHT activity (except in the no-flux experiment S3), and the intensification process is similar to that in the control experiment.

6. Conclusions

On the evidence presented above, we conclude that the inner-core flow asymmetries in a tropical cyclone are random and intrinsically unpredictable. This lack of predictability is a reflection of the convective nature of the inner-core region, and extends to the prediction of intensity itself. Deep convective towers growing in the rotation-rich environment of the incipient core amplify the local vertical rotation. These so-called 'vortical hot towers' (VHTs) are the basic coherent structures of the intensification process, which itself is intrinsically asymmetric and random in nature. In the numerical experiments presented herein, it is the progressive segregation, merger and axisymmetrization of these towers and the low-level convergence they generate that is fundamental to the intensification process, but axisymmetrization is never complete. There is always a prominent low-azimuthal-wave-number asymmetry (often for wave number 1 or 2) in the inner-core relative vorticity.

The WISHE feedback mechanism that has previously been proposed to explain tropical-cyclone intensification in an axisymmetric framework has been found to be much less of a constraint in three dimensions. We surmise that this is partly because the VHTs are able to extract surface moisture fluxes that are locally sufficient for their growth without the wind–moisture feedback that typifies WISHE. The tendency of the simulated hurricane intensity to surpass its predicted upper bound at high resolution has been verified here using the simplest explicit latent-heating scheme, with instantaneous rain fallout (pseudo-adiabatic dynamics).

Finally, even though the effect of β imposes a wave-number-1 forcing of the flow asymmetries and concomitant northwestward vortex motion, the inner-core behaviour is essentially the same as that on the f-plane, and again dominated by VHTs and vortex Rossby waves.

Acknowledgements

This research was supported in part by Grant No. N00014-03-1-0185 from the US Office of Naval Research and by National Science Foundation Grants ATM-0715426, ATM-0649943, ATM-0649944, and ATM-0649946. The first author is grateful for travel support provided by the German Research Council (DFG) as part of the Project 'Improved quantitative precipitation forecasting in Vietnam'.

References

Bergeron T. 1950. Über der Mechanismus der ausgiebigen Niederschläge. *Ber. Deut. Wetterd.* **12**: 225–232.

Bister M, Emanuel K. 1997. The genesis of Hurricane Guillermo: TEXMEX analyses and a modeling study. *Mon. Weather Rev.* **125**: 2662–2682.

Black ML, Gamache JF, Marks FD, Samsury CE, Willoughby HE. 2002. Eastern Pacific Hurricanes Jimena of 1991 and Olivia of 1994: The effect of vertical shear on structure and intensity. *Mon. Weather Rev.* **130**: 2291–2312.

Blackwell KG. 2000. The evolution of Hurricane Danny (1997) at landfall: Doppler-observed eyewall replacement, vortex contraction/intensification, and low-level wind maxima. *Mon. Weather Rev.* **128**: 4002–4016.

Braun SA, Tao W-K. 2000. Sensitivity of high-resolution simulations of hurricane Bob (1991) to planetary boundary layer parameterizations. *Mon. Weather Rev.* **128**: 3941–3961.

Braun SA. 2002. A cloud-resolving simulation of Hurricane Bob (1991): Storm structure and eyewall buoyancy. *Mon. Weather Rev.* **130**: 1573–1592.

Braun SA, Montgomery MT, Puc Z. 2006. High-resolution simulation of Hurricane Bonnie (1998). Part I: The organization of eyewall vertical motion. *J. Atmos. Sci.* **63**: 19–42.

Chen Y, Yau MK. 2001. Spiral bands in a simulated hurricane. Part I: vortex Rossby wave verification. *J. Atmos. Sci.* **58**: 2128–2145.

Chen Y, Brunet G, Yau MK. 2003. Spiral bands in a simulated hurricane. Part II: Wave activity diagnostics. *J. Atmos. Sci.* **60**: 1239–1256.

Davis CA, Bosart LF. 2002. Numerical simulations of the genesis of Hurricane Diana (1984). Part II: Sensitivity of track and intensity prediction. *Mon. Weather Rev.* **130**: 1100–1124.

Dengler K, Reeder MJ. 1997. The effects of convection and baroclinicity on the motion of tropical-cyclone-like vortices. *Q. J. R. Meteorol. Soc.* **123**: 699–727.

Dudhia J. 1993. A non-hydrostatic version of the Penn State–NCAR mesoscale model: Validation tests and simulation of an Atlantic cyclone and cold front. *Mon. Weather Rev.* **121**: 1493–1513.

Eliassen A, Lystad M. 1977. The Ekman layer of a circular vortex: A numerical and theoretical study. *Geophys. Norv.* **31**: 1–16.

Emanuel KA. 1989. The finite amplitude nature of tropical cyclogenesis. *J. Atmos. Sci.* **46**: 3431–3456.

DOI: 10.1002/qj

Emanuel KA. 1995. Sensitivity of tropical cyclones to surface exchange coefficients and a revised steady-state model incorporating eye dynamics. *J. Atmos. Sci.* **52**: 3969–3976.
Enagonio J, Montgomery MT. 2001. Tropical cyclogenesis via convectively forced vortex Rossby waves in a shallow water primitive equation model. *J. Atmos. Sci.* **57**: 685–706.
Fiorino M, Elsberry RL. 1989. Some aspects of vortex structure related to tropical cyclone motion. *J. Atmos. Sci.* **46**: 975–990.
Flatau M, Schubert WH, Stevens DE. 1994. The role of baroclinic processes in tropical cyclone motion: The influence of vertical tilt. *J. Atmos. Sci.* **51**: 2589–2601.
Frank WM, Ritchie EA. 1999. Effects of environmental flow upon tropical cyclone structure. *Mon. Weather Rev.* **127**: 2044–2061.
Frank WM, Ritchie EA. 2001. Effects of vertical wind shear on hurricane intensity and structure. *Mon. Weather Rev.* **129**: 2249–2269.
Grell GA, Dudhia J, Stauffer DR. 1995. 'A description of the fifth generation Penn State/NCAR mesoscale model (MM5)'. NCAR Tech. Note NCAR/TN-398+STR, 138 pp.
Hausman SA, Ooyama KV, Schubert WH. 2006. Potential vorticity structure of simulated hurricanes. *J. Atmos. Sci.* **63**: 87–108.
Hendricks EA, Montgomery MT, Davis CA. 2004. On the role of 'vortical' hot towers in formation of tropical cyclone Diana (1984). *J. Atmos. Sci.* **61**: 1209–1232.
Heymsfield GM, Halverson JB, Simpson J, Tian L, Paul Bui T. 2001. ER-2 Doppler radar investigations of the eyewall of Hurricane Bonnie during the Convection and Moisture Experiment-3. *J. Appl. Meteorol.* **40**: 1310–1330.
Hsie E-Y, Anthes RA, Keyser D. 1984. Numerical simulation of frontogenesis in a moist atmosphere. *J. Atmos. Sci.* **41**: 2581–2594.
Jones SC. 1995. The evolution of vortices in vertical shear. Part I: Initially barotropic vortices. *Q. J. R. Meteorol. Soc.* **121**: 821–851.
Jordan CL. 1958. Mean soundings for the West Indies area. *J. Meteor.* **15**: 91–97.
Kimball SK, Dougherty FC. 2006. The sensitivity of idealized hurricane structure and development to the distribution of vertical levels in MM5. *Mon. Weather Rev.* **134**: 1987–2008.
Kossin JP, Schubert WH. 2001. Mesovortices, polygonal flow patterns, and rapid pressure falls in hurricane-like vortices. *J. Atmos. Sci.* **58**: 2196–2209.
Kurihara Y, Bender M, Tuleya R, Ross R. 1990. Prediction experiments of Hurricane Gloria (1985) using a multiply nested movable mesh model. *Mon. Weather Rev.* **118**: 2185–2198.
Kwok HY, Chan JCL. 2005. The influence of uniform flow on tropical cyclone intensity change. *J. Atmos. Sci.* **62**: 3193–3212.
Lorenz EN. 1969. The predictability of a flow which possesses many scales of motion. *Tellus* **21**: 289–307.
Marks FD, Houze RA. 1984. Airborne Doppler radar observations in Hurricane Debby. *Bull. Am. Meteorol. Soc.* **65**: 569–582.
McWilliams JC, Flierl GR. 1979. On the evolution of isolated nonlinear vortices. *J. Phys. Oceanogr.* **9**: 1155–1182.
Möller JD, Montgomery MT. 1999. Vortex Rossby waves and hurricane intensification in a barotropic model. *J. Atmos. Sci.* **56**: 1674–1687.
Möller JD, Montgomery MT. 2000. Tropical cyclone evolution via potential vorticity anomalies in a three-dimensional balance model. *J. Atmos. Sci.* **57**: 3366–3387.
Montgomery MT, Enagonio J. 1998. Tropical cyclogenesis via convectively forced vortex Rossby waves in a three-dimensional quasi-geostrophic model. *J. Atmos. Sci.* **55**: 3176–3207.
Montgomery MT, Kallenbach RJ. 1997. A theory for vortex Rossby waves and its application to spiral bands and intensity changes in hurricanes. *Q. J. R. Meteorol. Soc.* **123**: 435–465.
Montgomery MT, Vladimirov VA, Denissenko PV. 2002. An experimental study on hurricane mesovortices. *J. Fluid Mech.* **471**: 1–32.
Montgomery MT, Nicholls ME, Cram TA, Saunders AB. 2006a. A vortical hot tower route to tropical cyclogenesis. *J. Atmos. Sci.* **63**: 355–386.
Montgomery MT, Bell MM, Aberson SD, Black ML. 2006b. Hurricane Isabel (2003): New insights into the physics of intense storms. Part I: Mean vortex structure and maximum intensity estimates. *Bull. Am. Meteorol. Soc.* **87**: 1335–1348.
Musgrave KD, Davis CA, Montgomery MT. 2008. Numerical simulations of the formation of hurricane Gabrielle (2001). *Mon. Weather Rev.* (in press).
Nguyen CM, Smith RK, Zhu H, Ulrich W. 2002. A minimal axisymmetric hurricane model. *Q. J. R. Meteorol. Soc.* **128**: 2641–2661.
Nolan DS. 2001. The stabilizing effects of axial stretching on turbulent vortex dynamics. *Phys. Fluids* **13**: 1724–1738.
Ooyama KV. 1969. Numerical simulation of the life cycle of tropical cyclones. *J. Atmos. Sci.* **26**: 3–40.
Peng MS, Jeng B-F, Williams RT. 1999. A numerical study on tropical cyclone intensification. Part I: Beta effect and mean flow effect. *J. Atmos. Sci.* **56**: 1404–1423.
Persing J, Montgomery MT. 2003. Hurricane superintensity. *J. Atmos. Sci.* **60**: 2349–2371.
Raymond DJ, Jiang H. 1990. A theory for long-lived mesoscale convective systems. *J. Atmos. Sci.* **47**: 3067–3077.
Raymond DJ, López-Carrillo C, López Cavazos L. 1998. Case-studies of developing east Pacific easterly waves. *Q. J. R. Meteorol. Soc.* **124**: 2005–2034.
Reasor PD, Montgomery MT, Marks FD, Gamache JF. 2000. Low-wavenumber structure and evolution of the hurricane inner core observed by airborne dual-Doppler radar. *Mon. Weather Rev.* **128**: 1653–1680.
Reasor PD. Montgomery MT, Grasso LD. 2004. A new look at the problem of tropical cyclones in vertical shear flow: Vortex resiliency. *J. Atmos. Sci.* **60**: 97–116.
Riehl H, Malkus JS. 1958. On the heat balance in the equatorial trough zone. *Geophysica* **6**: 503–538.
Ritchie EA, Frank WM. 2007. Interactions between simulated tropical cyclones and an environment with a variable Coriolis parameter. *Mon. Weather Rev.* **135**: 1889–1905.
Rogers R, Chen S, Tenerelli J, Willoughby H. 2003. A numerical study of the impact of vertical shear on the distribution of rainfall in hurricane Bonnie (1998). *Mon. Weather Rev.* **131**: 1577–1599.
Rogers RF, Fritsch JM. 2001. Surface cyclogenesis from convectively driven amplification of midlevel mesoscale convective vortices. *Mon. Weather Rev.* **129**: 605–637.
Rotunno R, Emanuel KA. 1987. An air–sea interaction theory for tropical cyclones. Part II: Evolutionary study using a nonhydrostatic axisymmetric numerical model. *J. Atmos. Sci.* **44**: 542–561.
Schecter DA, Dubin DHE. 1999. Vortex motion driven by a background vorticity gradient. *Phys. Rev. Lett.* **83**: 2191–2194.
Schecter DA, Montgomery MT. 2003. On the symmetrization rate of an intense geophysical vortex. *Dyn. Atmos. Oceans* **37**: 55–88.
Schecter DA, Montgomery MT. 2007. Waves in a cloudy vortex. *J. Atmos. Sci.* **64**: 314–337.
Schubert WH, Montgomery MT, Taft RK, Guinn TA, Fulton SR, Kossin JP, Edwards JP. 1999. Polygonal eyewalls, asymmetric eye contraction, and potential vorticity mixing in hurricanes. *J. Atmos. Sci.* **56**: 1197–1223.
Simpson J, Halverson JB, Ferrier BS, Petersen WA, Simpson RH, Blakeslee R, Durden SL. 1998. On the role of 'hot towers' in tropical cyclone formation. *Meteorol. Atmos. Phys.* **67**: 15–35.
Smith RK. 1968. The surface boundary layer of a hurricane. *Tellus* **20**: 473–484.
Smith RK. 2006. Accurate determination of a balanced axisymmetric vortex. *Tellus* **58A**: 98–103.
Smith RK, Ulrich W. 1990. An analytical theory of tropical cyclone motion using a barotropic model. *J. Atmos. Sci.* **47**: 1973–1986.
Smith RK, Weber HC. 1993. An extended analytic theory of tropical cyclone motion. *Q. J. R. Meteorol. Soc.* **119**: 1149–1166.
Trier SB, Davis CA, Skamarock WC. 2000. Long-lived mesoconvective vortices and their environment. Part II: Induced thermodynamic destabilization in idealized simulations. *Mon. Weather Rev.* **128**: 3396–3412.
Wang Y, Holland GJ. 1996a. The beta drift of baroclinic vortices. Part II: Diabatic vortices. *J. Atmos. Sci.* **53**: 3737–3756.
Wang Y, Holland GJ. 1996b. The beta drift of baroclinic vortices. Part I: Adiabatic vortices. *J. Atmos. Sci.* **53**: 411–427.
Wang Y. 2001. An explicit simulation of tropical cyclones with a triply nested movable mesh primitive equation model: TCM3. Part I: Model description and control experiment. *Mon. Weather Rev.* **129**: 1370–1394.
Wang Y. 2002a. Vortex Rossby waves in a numerical simulated tropical cyclone. Part I: Overall structure, potential vorticity, and kinetic energy budgets. *J. Atmos. Sci.* **59**: 1213–1238.
Wang Y. 2002b. Vortex Rossby waves in a numerical simulated tropical cyclone. Part II: The role in tropical cyclone structure and intensity changes. *J. Atmos. Sci.* **59**: 1239–1262.
Weckwerth TM. 2000. The effect of small-scale moisture variability on thunderstorm initiation. *Mon. Weather Rev.* **128**: 4017–4030.
Willoughby HE, Jin H-L, Lord SJ, Piotrowicz JM. 1984. Hurricane structure and evolution as simulated by an axisymmetric, nonhydrostatic numerical model. *J. Atmos. Sci.* **41**: 1169–1186.

DOI: 10.1002/qj

Wu L, Braun SA. 2004. Effects of environmentally induced asymmetries on hurricane intensity: A numerical study. *J. Atmos. Sci.* **61**: 3065–3081.
Zhu H, Smith RK. 2002. The importance of three physical processes in a three-dimensional tropical cyclone model. *J. Atmos. Sci.* **59**: 1825–1840.
Zhu H, Smith RK. 2003. Effects of vertical differencing in a minimal hurricane model. *Q. J. R. Meteorol. Soc.* **129**: 1051–1069.
Zhu H. Smith RK, Ulrich W. 2001. A minimal three-dimensional tropical cyclone model. *J. Atmos. Sci.* **58**: 1924–1944.
Zipser EJ, Gautier C. 1978. Mesoscale events within a GATE tropical depression. *Mon. Weather Rev.* **106**: 789–805.

DOI: 10.1002/qj